Measurement 235 (2024) 114988

Contents lists available at ScienceDirect

Measurement

journal homepage: www.elsevier.com/locate/measurement

Laser-textured cross-hatched surface topography analysis with evaluation of high-frequency measurement noise

Przemysław Podulka [a,*], Wojciech Macek [b], Ricardo Branco [c], Andrzej Kubit [a]

[a] Faculty of Mechanical Engineering and Aeronautics, Rzeszow University of Technology, Powstancow Warszawy 12, 35-959 Rzeszów, Poland
[b] Faculty of Mechanical Engineering and Ship Technology, Gdańsk University of Technology, Narutowicza 11/12, 80-233 Gdańsk, Poland
[c] CEMMPRE, ARISE, Department of Mechanical Engineering, University of Coimbra, 3030-788 Coimbra, Portugal

ARTICLE INFO

Keywords:
Surface topography
Surface texture
Roughness
Measurement noise
Texture direction
Laser texturing
Cross-hatch texture

ABSTRACT

The precision of surface roughness determination using ISO 25178 parameters relies on various factors that directly impact the measurement process. In industry applications, the contactless roughness measurement reduces data collection time. However, it introduces several potential errors, including those stemming from the environment. One of the main types of errors encountered during topography analysis is measurement noise, which arises from different external disturbances. High-frequency noise is particularly studied as a result of vibration. In the present study, the laser-texture cross-hatched surface topographies were analysed using the results obtained from white light interference measurements. Measurement noise was defined based on noisy data, also called noise surface, which is the result of filter decomposition methods. This data separation technique was supported with power spectral analysis, autocorrelation function applications and texture direction characterisation. It was suggested to conduct a comprehensive study of the noisy data to enhance the understanding of texturing direction. Various data filtration techniques were studied, namely robust Gaussian, spline, fast Fourier transform and morphological closing-opening filters. The results of the proposed procedure were validated against variations in the values of ISO 25178 surface texture parameters. Validating the proposed approach, the variations of noise-sensitive surface texture parameters were compared to the variations of the same parameters but received by averaging three repeated measurements, as proposed by international standards. The main advantage of the proposed method against standards procedure was reducing the time of data collection when the measurement must be repeated and averaged. In conclusion, a method for reducing high-frequency measurement noise was introduced through the application of the proposed procedure.

1. Introduction

Surface topography, which can be decomposed to the shape, waviness and roughness [1], is formed during the last stage of the machining process. A detailed analysis of this data can provide important and valuable information can be received, such as insights into lubricant retention [2] or friction behaviour [3] in tribological performance, damage of crystal materials [4], description of fatigue test results [5], cavitation erosion assessments [6], friction torque modelling [7] or surface properties prediction by data simulation [8]. When selecting a proper surface texture parameter, its study can deliver information on which parameters should be monitored throughout the entire manufacturing process [9].

Measurements of surface topography were found to be of great significance in the characterisation of laser-textured surfaces, as reviewed by Etison [10]. Patel et al. [11] studied the micro-texturing process of Ti6Al4V material for various wetting times of the material surface. Riveiro et al. [12] characterised polymers for biomedical applications based on an extensive analysis of laser surface texturing. Wahab et al. [13] reviewed different approaches to enhance the material performance during surface texturing, such as abrasive blasting, reactive-ion etching, lithography, and mechanical machining. Fang et al. [14] analysed the use of ultra-short pulse laser treatments in honing applications. Voevodin et al. [15] reduced friction and wear under variable environmental conditions using solid lubricant systems in precision laser machining. Moreover, Lutey et al. [16] studied adhesion and wettability for pulsed laser machining based on areal surface roughness and

* Corresponding author.
E-mail addresses: p.podulka@prz.edu.pl (P. Podulka), wojciech.macek@pg.edu.pl (W. Macek), ricardo.branco@dem.uc.pt (R. Branco), akubit@prz.edu.pl (A. Kubit).

https://doi.org/10.1016/j.measurement.2024.114988
Received 3 January 2024; Received in revised form 25 April 2024; Accepted 21 May 2024
Available online 23 May 2024

Nomenclature

α	cross-hatch angle
β_1, β_2, β_3, β_4	angles defined for the directions of profile extractions
ACF	autocorrelation function
FFTF	fast Fourier transform filter
LSPL	least-square plane data levelling method
MOF	morphological filter
NMPs	non-measured points
NS	noise surface, noisy data
PSD	power spectral density
RGRF	robust Gaussian regression filter
SF	regular isotropic spline filter
TD	texture direction
WLI	white light interferometry
Sa	arithmetic mean height, μm
Sal	auto-correlation length, mm
Sbi	surface bearing index
Sci	core fluid retention index
Sdq	root mean square gradient
Sdr	developed interfacial areal ratio, %
Sk	core roughness depth, μm
Sku	kurtosis
Smc	inverse areal material ratio, μm
Smr	areal material ratio, %
Sp	maximum peak height, μm
Sp/Sz	emptiness coefficient
Spc	arithmetic mean peak curvature, 1/mm
Spd	peak density, 1/mm^2
Spk	reduced summit height, μm
Sq	root mean square height, μm
Sr1	upper bearing area, %
Sr2	lower bearing area, %
Ssk	skewness
Std	texture direction, °
Str	texture parameter
Sxp	extreme peak height, μm
Sv	maximum valley depth, μm
Svi	valley fluid retention index
Svk	reduced valley depth, μm
Sz	the maximum height of the surface, μm
Vm	material volume, μm^3/μm^2
Vmc	core material volume, μm^3/μm^2
Vmp	peak material volume, μm^3/μm^2
Vv	void volume, μm^3/μm^2
Vvc	core void volume, μm^3/μm^2
Vvv	pit void volume, μm^3/μm^2

ablation depth.

Laser texturing of surfaces has tremendous potential in biomedical applications [17]. Tiainen et al. [18] improved the primary stability and the osseointegration process of dental implants using a novel laser texturing method. Cunha et al. [19] demonstrated that surface modification by laser irradiation of zirconia dental implants can enhance surface topographic aspects. According to Khatami et al. [20], nanoscale texturing can strengthen both the physical and chemical properties of dental implants. Mukherjee et al. [21] explored the relationship between surface chemistry, laser-texturing topography and the behaviour of the cells in pattern recognition and characterisation. The importance of surface texturing for bone integration based on photolithography studies was addressed by Hallgren et al. in [22]. Menci et al. [23] studied the influence of variations in wavelength and pulse duration of the laser texturing process on the characterisation of orthopaedic applications.

Considering a vast number of studies on surface laser treatment, many advantages have been identified. However, an accurate description of the surface topography of textured surfaces depends on different aspects. An important aspect is a measurement noise associated with a specified frequency. Generally, the measurement noise is defined as an additional noise in the output signal during normal use of the measuring instrument [24]. In many cases, the characterisation of measurement noise considers its bandwidth. Additionally, when studying 'noise density', a widely discussed issue is high-frequency errors [25].

Reduction in errors caused by measurement noise can be attained by repeating the surface measuring process [26]. Although this is an encouraging solution, industrial applications aim to reduce the measuring time while controlling the manufacturing process [27]. To meet these requirements, the characterisation of high-frequency noise has been proposed through studies focused on 'noisy data', which encompasses the application of a digital filter to separate data based on its frequency [28]. Gaussian filters are among the most commonly used, especially for surface metrology analysis of additively manufactured materials [29,30]. From a historical perspective, Gaussian filters have been comprehensively studied and standardised over the years considering diverse metrological issues [31,32] and their functional appliances. Advancements in surface filtering have been proposed with robust modifications of the classical Gaussian approach [33] which was more insensitive to outliers.

Another limitation in surface roughness data filtering is associated with spline interpolation. Chen et al. [34] addressed different spline interpolation approaches for modelling and simulating surface topographies in ball-end milling processes. Podulka [35] compared various spline filtering techniques to reduce high-frequency errors in the evaluation of machined components. Janecki [36] studied the separation of both areal surface topography waviness and roughness through a two-dimensional isotropic spline filter with an improved response relative to end effects. An areal spline filter with isotropy obtained by approximating the transmission characteristic of the Gaussian filter was used by Tong et al. [37]. They proposed a weighting factor to mitigate end-effect issues by employing new boundary conditions. Gogolewski [38] applied fractional spline techniques for diagnosing surface texture in engineering materials fabricated by additive manufacturing and face milling.

He et al. [39] conducted an extensive analysis of the frequency spectrum of topography data by fast Fourier transform to evaluate the asperity radius of curvature and the asperity density. The measurement of thin film surface roughness with optical appliances was also improved using a fast Fourier transform, as demonstrated by Tien et al. [40]. Jiang et al. [41] used a fast Fourier transform to quantify the similarity of surface topographies, determining whether they were created from the same measured data. Dong et al. [42] utilised a Wiener filter Fourier transform to accurately reconstruct microstructures with a large slope considering white light interference surface topography measurements. Podulka [43] identified selected types of errors occurring in white light interference measurements of plateau-honed cylinder liner surfaces. Guo et al. [44] applied non-uniform fast Fourier transforms to determine the optical homogeneity of parallel plates in interference metrology.

Relevant information on surface roughness was obtained via the application of morphological filters, such as those described in the ISO 16610-85 standard [45]. Lou et al. [46] compared mean-line-based filters with morphological operations. They concluded that the former, as functions-oriented, were more appropriate for functional prediction of component performance [47]. The same authors improved the definition of true tribological contact through the characterisation of surface topography using morphological methods [48]. Morphological dilation and erosion were applied by Newton et al. [49] to improve segmentation

in edge-data analysis. Lipiński et al. [50] utilised a structural disc-shaped envelope opening method as a reconstruction operation to detect abrasive grain tips. Podulka [51] compared envelope morphological filtration with regular algorithms and reported significant advantages in surface texture assessment.

Although there are numerous algorithms for filtration of surface roughness, there are still several unsolved issues, such as errors caused by vibrations. Thus, it is crucial to provide appropriate guidance on how to apply digital noise-suppression filters, particularly considering the high number of digital operations involved in typical roughness data analysis processes, which include levelling, outliers removal and reduction of measurement errors. High-frequency noise can significantly influence the values of ISO 25178 surface texture parameters obtained for laser-textured cross-hatched surfaces. In the present study, it is proposed a procedure which incorporates autocorrelation, power spectral and direction functions. The effectiveness of the proposed procedure is validated by accounting for the variations of ISO 25178 surface texture parameters.

2. Materials and methods

2.1. Analysed surfaces

This study analyses laser-textured surfaces treated with cross-hatching at various angles. The cross-hatching technique was found to be crucial in addressing several tribological problems, such as starved hydrodynamic linear contact mechanics [52]. A cross-hatch strategy with angles ranging from 0 to 90 degrees was utilised by Ozan et al. [53] for the characterisation of laser-textured alloys in biomedical applications. Guimarães et al. [54] obtained micropatterns in WC-Co green compacts with a contact angle of 30° which resulted in a 27 % reduction in the wettability of the cutting tools.

Laser-textured surfaces with cross-hatch patterns can reduce friction under lubricated conditions [55]. In Hank's solution, the texturing with crosshatching presented encouraged frictional characteristics once the surfaces have undergone a running-in period. In addition, it facilitates the removal of the bulges found in the vicinity of the laser traces, particularly in dry conditions [56]. It was also hypothesized that the formation of a thick resolidified passive oxide layer after laser-texturing with cross-hatched paths contributed to the enhancement of corrosion

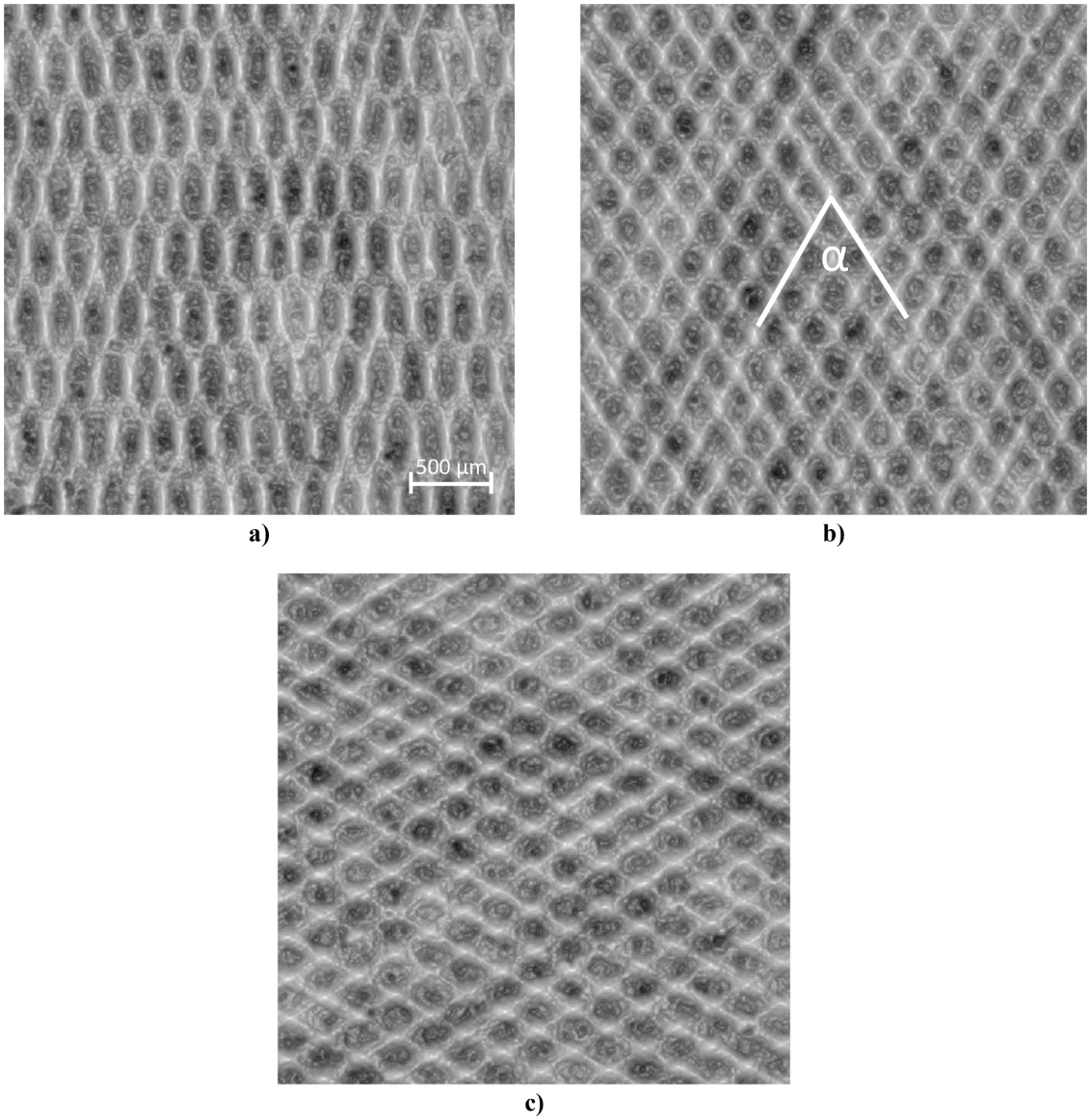

Fig. 1. Images of laser textured surfaces with a cross-hatch angle (α) equal to: α = 30° (a), α = 60° (b) and α = 120° (c).

and tribocorrosion properties [57].

In the current research, the cross-hatch angle, represented by the α value, was set to 30°, 60°, 90°, 120°, and 150°. The laser machining involved using a 20 W ytterbium pulse device with energy and duration equal to 1 mJ and 2 ns, respectively. The repetition rate was 1000 kHz, the focal diameter was around 60 μm and the beam-driven path was built on the mentioned cross-hatched angles, correspondingly. The marking speed was 100 mm/s. The effect of main laser-texturing parameters on the tribological properties of coatings was widely studied by Giorleo et al. [58].

More than 10 surfaces for each type of cross-hatch angle were comprehensively studied. The differences in ISO 25178 surface texture parameters were analysed and described with a relative difference for each one of them. The results were also studied in terms of statistical performance, and the final results were interpreted in the discussion section considering the medium values.

Fig. 1 exhibits several examples of laser-textured surfaces with an α value equal to 30° (a), 60° (b) and 120° (c). The cross-hatch angle α is also schematised in Fig. 1(b).

2.2. Measurement process and surface texture parameters

The surface topography was obtained from the workpieces using a contactless white light interference (WLI) instrument Talysurf CCI Lite. The height resolution was 0.01 nm, and the measured area was 3.35 mm × 3.35 mm, capturing 1024 × 1024 data points. The spacing between the points was 3.27 μm and a Nikon (5×/0.13 TI) objective was used for all measurements of the tested specimens. Around 20 topographies for each cross-hatch angle (i.e., $\alpha = 30°$, $\alpha = 60°$, $\alpha = 90°$, $\alpha = 120°$ and $\alpha = 150°$) were studied. All of the measurements were repeated three times to determine the mean value aiming to validate the procedure according to the raw measured data.

The ISO 25178 surface texture parameters were calculated with TalyMap Gold software from Digital Surf company. The same software was utilised for the evaluation of power spectral density (PSD), auto-correlation function (ACF) and texture direction (TD) graph, which were considered for areal and profile performances.

The raw measured data were subjected to pre-processing, including fulfilling non-measured points (NMPs), data levelling and outlier removal. NMPs were fulfilled by using a smooth shape calculated from the neighbouring points. Data levelling was carried out through the least square plane (LSPL) method considering the evaluation of the entire area. Finally, outliers were removed by employing the hard data thresholding technique, with values defined in the interval 0.13 % – 99.87 %, as defined in previous studies [59]. The flow chart of the pre-processing procedure is presented in Fig. 2.

Fig. 3 exhibits different isometric views, surface texture parameters and extracted random horizontal profiles of laser-textured surfaces with cross-hatch angles (α) of 30° and 90°. The analysis encompassed different groups of ISO 25178 surface texture parameters, namely height (amplitude), functional, spatial, hybrid, volume functional, feature, material ratio curves and functional indices. The variations in topography parameters from the above-mentioned groups were studied to better understand the reduction process of high-frequency measurement noise.

2.3. Applied methods for the data processing and roughness evaluation improvements

In order to improve the suppression of high-frequency measurement errors, a detailed analysis of noise data was proposed. The noisy data was defined as data removed after initial assessments as part of the pre-processing of the raw measured data. This noisy data is generally called noise surface (NS) [28]. This task aimed to separate high-frequency components from the pre-processed data, ensuring that the removed noisy data contained only the components of the desired frequency or, at least, that this frequency is dominant. Fig. 4 presents several examples of noisy data extraction (noise surface) with isometric views focused on laser-textured cross-hatched surfaces with an angle of $\alpha = 60°$. The filtering process was carried out by applying a regular isotropic 5 μm robust Gaussian regression filter.

In some cases, the selection of the filtering method for high-frequency noise suppression was improved by thresholding the noisy data [60]. Considering the isotropic properties of the NS, the noisy data is more isotropic when it does not contain non-noise features. It was found that the number of treatment traces on the NS decreased as the isotropy of noisy data increased [61].

The detection of non-noise patterns on the NS was improved by both thresholding of the noisy data and, additionally, by thresholding of the ACF calculated for an NS. For the study of laser-textured cross-hatched surfaces, it was found that thresholding of NS data did not always allow restriction if the noisy data contained non-noise patterns. Fig. 5 shows an example of NS thresholding along with a description of the value selection (A1 and A2). Therefore, thresholding was used for ACF data, as demonstrated in Fig. 6. The non-noise features were easily detected in the thresholded ACF data.

Fig. 7 displays isometric views of a WLI-measured laser-textured cross-hatched surface for a cross-hatch angle (α) of 60° after the application of both 7.5 μm robust Gaussian regression (a) and spline (b) filtering approaches. A spectral analysis of the NS, as represented by the

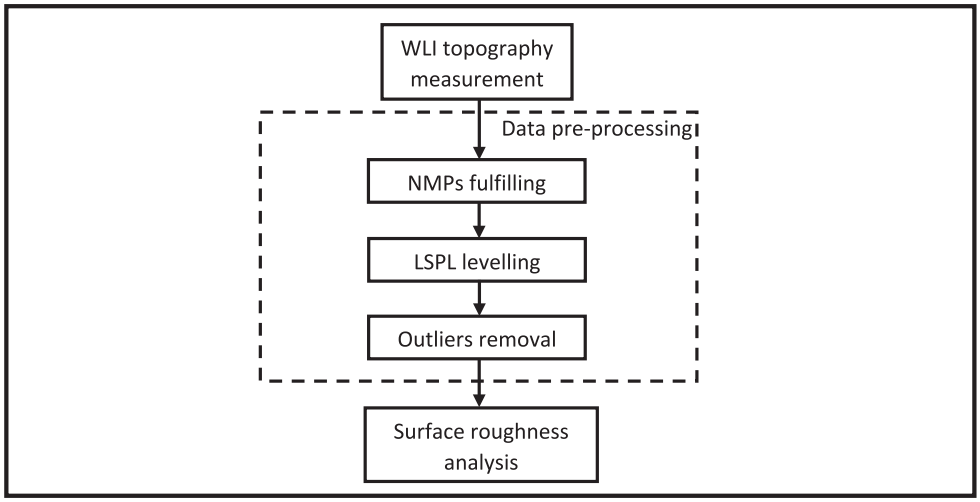

Fig. 2. The flow chart of the WLI raw measured data pre-processing procedure.

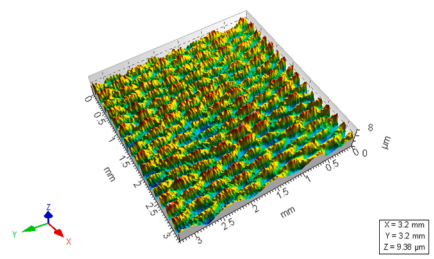

a)

Sq = 1.4 µm, Ssk = 0.00675, Sku = 2.56,
Sp = 4.89 µm, Sv = 4.48 µm,
Sz = 9.38 µm, Sa = 1.14 µm,
Smr = 0.0890 %, Smc = 3.05 µm,
Sxp = 2.70 µm,
Sal = 0.0468 mm, Str = 0.281, Std = 76.0 °,
Sdq = 0.0863, Sdr 0.372 %,
Vm = 0.0000575 mm^3/mm^2,
Vv = 0.00190 mm^3/mm^2,
Vmp = 0.0000575 mm^3/mm^2,
Vmc = 0.00133 mm^3/mm^2,
Vvc = 0.00175 mm^3/mm^2,
Vvv = 0.000150 mm^3/mm^2,
Spd = 71 $1/mm^2$, Spc = 0.0363 1/mm,
Sk = 3.85 µm, Spk = 0.940 µm, Svk = 1.06 µm,
Sr1 = 8.44 %, Sr2 = 90.2 %,
Sbi = 0.543, Sci = 1.56, Svi = 0.107

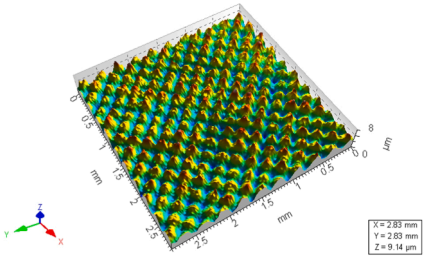

b)

Sq = 1.4 µm, Ssk = 0.03910, Sku = 2.56,
Sp = 4.92 µm, Sv = 4.22 µm,
Sz = 9.14 µm, Sa = 1.14 µm,
Smr = 0.0684 %, Smc = 3.05 µm,
Sxp = 2.66 µm,
Sal = 0.0608 mm, Str = 0.832, Std = 47.9 °,
Sdq = 0.0869, Sdr = 0.377 %,
Vm = 0.000058 mm^3/mm^2,
Vv = 0.00192 mm^3/mm^2,
Vmp = 0.0000580 mm^3/mm^2,
Vmc = 0.00132 mm^3/mm^2,
Vvc = 0.00178 mm^3/mm^2,
Vvv = 0.000148 mm^3/mm^2,
Spd = 52 $1/mm^2$, Spc = 0.0354 1/mm,
Sk = 3.98 µm, Spk = 0.937 µm, Svk = 1.02 µm,
Sr1 = 8.44 %, Sr2 = 91.0 %,
Sbi = 0.545, Sci = 1.58, Svi = 0.105

c)

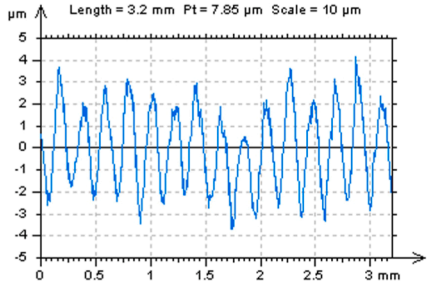

e)

d)

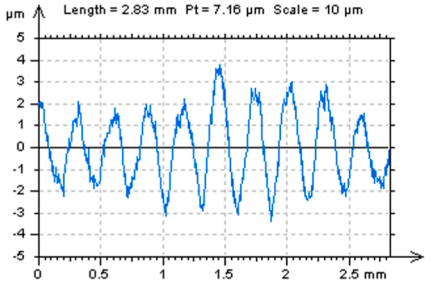

f)

Fig. 3. Isometric views of the laser-textured surfaces with cross-hatch angles (α) of 30° (a) and 90° (b), their ISO 25178 texture parameters (c,d) and horizontal profiles (e,f), respectively.

PSD function, showed that the implementation of the spline filter led to more high-frequency components compared to the robust Gaussian method. Moreover, the shape of the ACF function was also different, indicating the dominant presence of high-frequency data, as comprehensively studied by Podulka et al. [60]. Comparing both filtering methods, it was found that the most significant improvement was obtained with a 0.13 % – 99.87 % thresholding of the ACF data.

When characterising surface topographies with specified patterns, the direction of the machining traces can also be studied. Laser-textured cross-hatched surfaces exhibit topographies with two directions of treatment features, forming an angle α between them. Therefore, a comprehensive study of the NS data in the direction of machining can provide crucial insights into the isotropic properties of the noisy data. Fig. 8 presents the TD maps for NSs obtained using Gussian (a) and spline (b) filtering techniques, respectively. The isotropy, in both cases, was similar, approximately equal to 70.7 %. However, the first, second and third main directions of noisy data topographies were different. When extracting profiles in the first direction, 66° after robust Gaussian and 83° after spline filtering, considerable variations were obtained in the PSDs and ACFs. In contrast to the results obtained with the regular robust Gaussian filtering technique, the spline method emphasised the dominant high-frequency nature of the NS resulting in a more rapid increase of the maximum ACF value. Both the PSD and the ACF properties of the noisy data suggest that the spline filter is more effective encouraging than the robust Gaussian approach.

2.4. Proposed procedure for reduction of errors in the roughness characterisation

Fig. 9 presents the flow chart of the proposed procedure. Firstly, the WLI-measured surface topography data is subjected to a 3-step preprocessing procedure, described in the subsection devoted to the measurement process. Secondly, the reduction of high-frequency measurement noise is applied. In the last stage, the ISO surface texture parameters for laser-textured cross-hatched surfaces are evaluated.

The main goal of the proposed procedure is to minimise the influence of high-frequency errors through the analysis of noisy data, defined as noise surface (NS). Considering the features of NS obtained by filtration

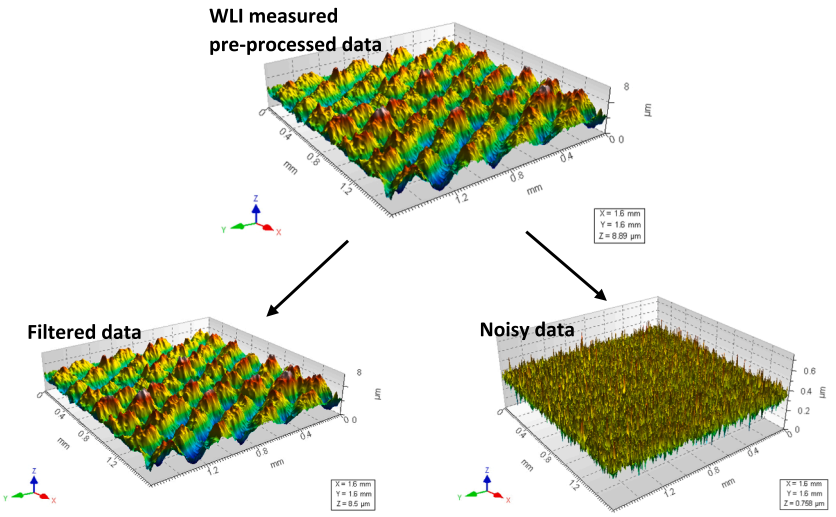

Fig. 4. Isometric view of the laser-textured surfaces with cross-hatch angle (α) of 60° subjected to the decomposition by using a 5 μm robust Gaussian regression filter.

of high-frequency noise, it is important to ensure that it only contains high-frequency components or, at least, they are predominant. It was found that well-received NS often consist of high-frequency noisy data, which can be characterised by the ower spectrum density function, often referred to PSD [62]. Alcock et al. [63] found a PSD function suitable for defining surface height error maps, particularly for optical surfaces. However, relying only on a single function for characterisation can may lack validation. Therefore, performing a simultaneous analysis of noisy data using more functions can provide more robust insights. Similarly, studying the shape of the ACF and ensuring that the NS exhibits isotropic properties are also pivotal considerations.

Assuming that the shape of autocorrelated data can influence the precision in generating of surface topography [64], the ACF has proven to be an efficient tool in detecting high-frequency data [60]. From the function characterisation, results show that the maximum value increases more rapidly compared to results that did not contain high-frequency components [65]. This property of ACF application can be particularly valuable in the study of stratified surfaces [66] with direction-oriented specifications. In addition to ensuring data isotropic properties, the texture direction characterisation, represented by the TD function, serves to validate if noisy data predominates in the direction of the surface finishing path. Texture direction was often defined as the 'level of isotropy' of surface topography data [67].

Thus, in the first part of the procedure, it is analysed the PSD, ACF and TD of the NS. Once the above conditions are met, profiles are extracted from the noisy data and subjected to a comprehensive analysis in the second part of the noise-removal approach. The analysis of the TD function allows us to determine the first, second and third dominant directions of the data. In the further surface assessments, the first direction is considered and is equal to the direction of the profile extraction. The differences can vary based on the applied filtering method and can help in the selection of the filtration algorithm and its bandwidth. For the frequency studies of the extracted profile data, the PSD and ACF characterisations are used, respectively.

The first dominant direction of noisy data should not align with the orientation of the surface machining, which suggests the removal of non-noise data components [60]. Revisiting the basis of the NS isotropic properties, similarly, the dominant direction of noisy data should not coincide with the orientation of the machining path, especially in laser-texturing processes. Therefore, the validation of the procedure was carried out with angles denoted as β_1, β_2, β_3, and β_4, and detailed described in subsequent sections.

Finally, the frequency properties of extracted β_1, β_2, β_3 and β_4 direction profiles are validated through the characterisation of the composition of data frequencies using both PSD and ACF functions. Upon confirming the adequacy of the direction, the filter selected and its bandwidth were classified as the most effective, among those studied, to reduce the high-frequency measurement noise.

3. Results and discussion

3.1. Application of texture direction function for the reduction of high-frequency measurement errors

To enhance the reduction of high-frequency measurement errors, PSD, ACF and TD functions were used simultaneously. The analysis of the contour map plots of the NS filtered through various techniques revealed the absence of non-noise patterns. Examples of the application of RGRF (a,b), SF (c,d), FFTF (e,f) and MOF (g,h) filtering methods are displayed in Fig. 10. As can be seen, there are visible differences associated with the spectral analysis, see Fig. 11. In addition, PSDs of NSs indicated encouraging results for the SF and FFTF approaches compared to RGRF and MOF methods with SF and FFTF retained more high-frequency data than other filtering schemes. The observation was better substantiated through the examination of the ACF shape. The NS values obtained by SF and FFTF methods increased more significantly near the maximum value than the two other techniques.

Further improvements were observed in the other two filtering approaches for the contour map plots of the thresholded NS data, as presented in Fig. 12. However, in this case, SF gained some advantage over NS created using FFTF filtering which allows the acquisition of noisy data without non-noise features. For the NS obtained via FFTF filtering, some directional patterns were recognized, as indicated by the arrows in Fig. 12e.

A significant enhancement was visible in the characterisation of TD graphs. The isotropy for the NS obtained by the FFTF filtering was markedly smaller (equal to 0 %) than the isotropy for the NS obtained with the SF filtering (equal to 70.7 %). The ratio of isotropy calculated for NS filtered by SF was equal to the ratio received for the NS obtained with the RGRF filtering. However, the NS filtered with RGRF contained non-noise patterns, as evident in the thresholded noisy data.

In addition to the proposed TD characterisation, the first direction of

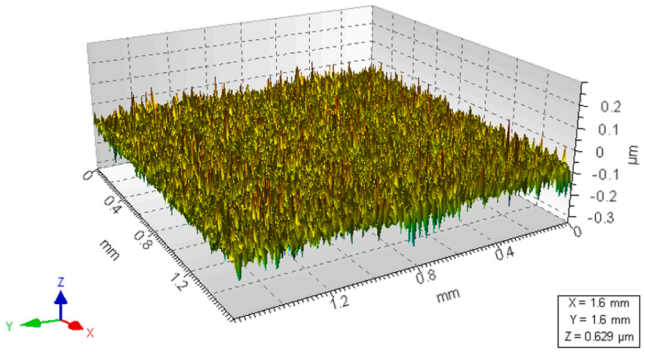

a)

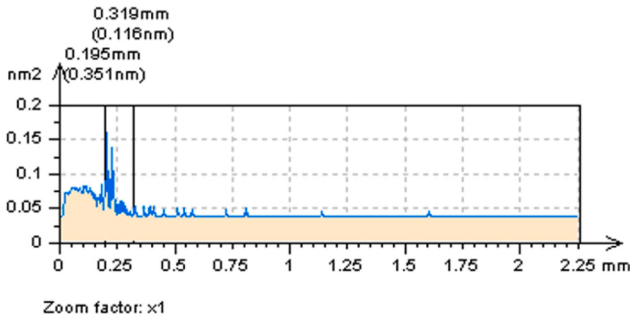

b)

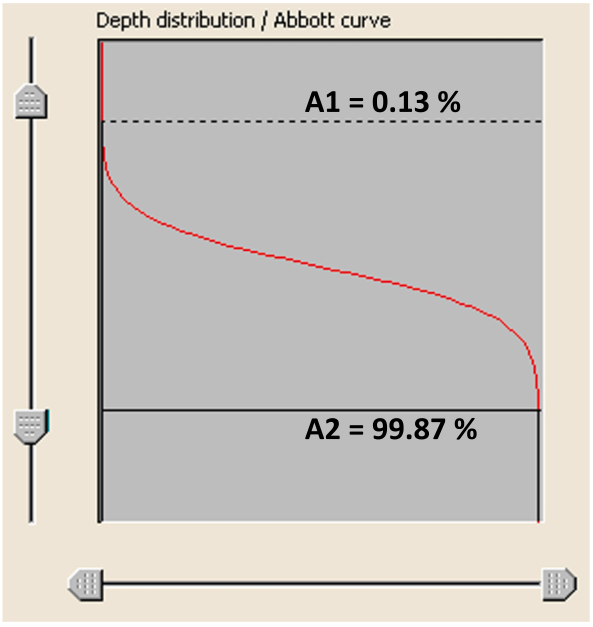

c)

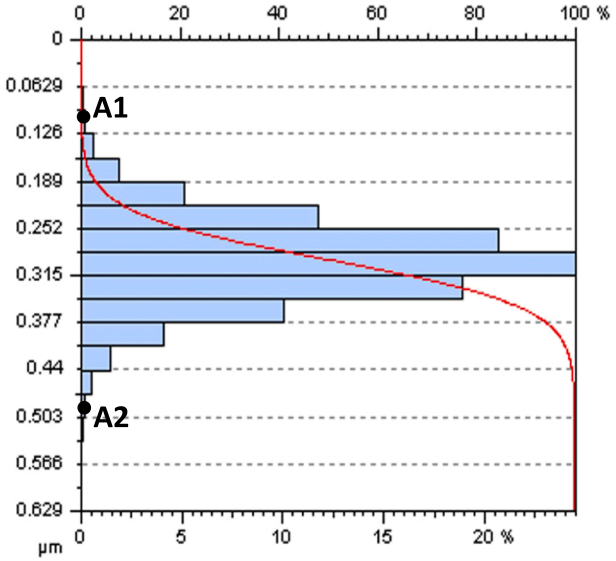

d)

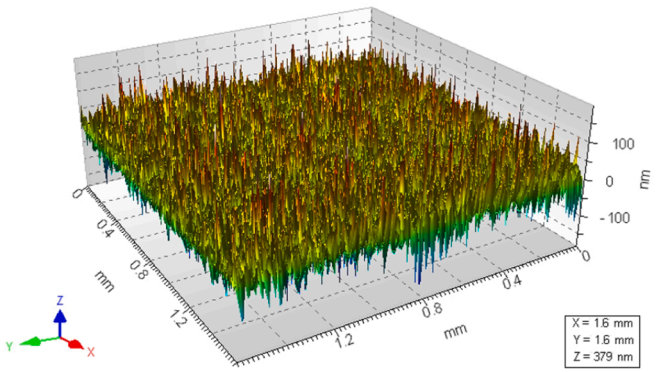

e)

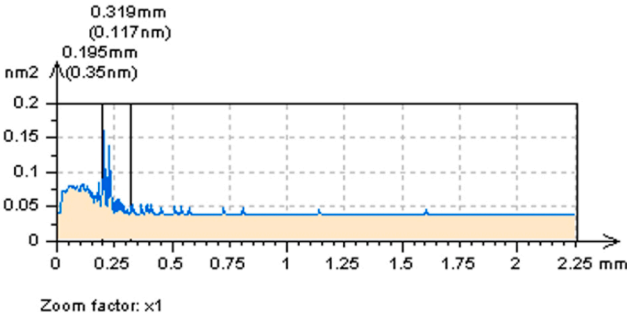

f)

Fig. 5. The isometric view of the NS obtained using a 7.5 µm robust Gaussian regression filter (a), its PSD (b), application of thresholding technique (c) with Abbott-Firestone curve analysis (d) and thresholded NS (e) with its PSD (f); received from WLI measured laser-textured cross-hatched surface with an angle (α) of 30°.

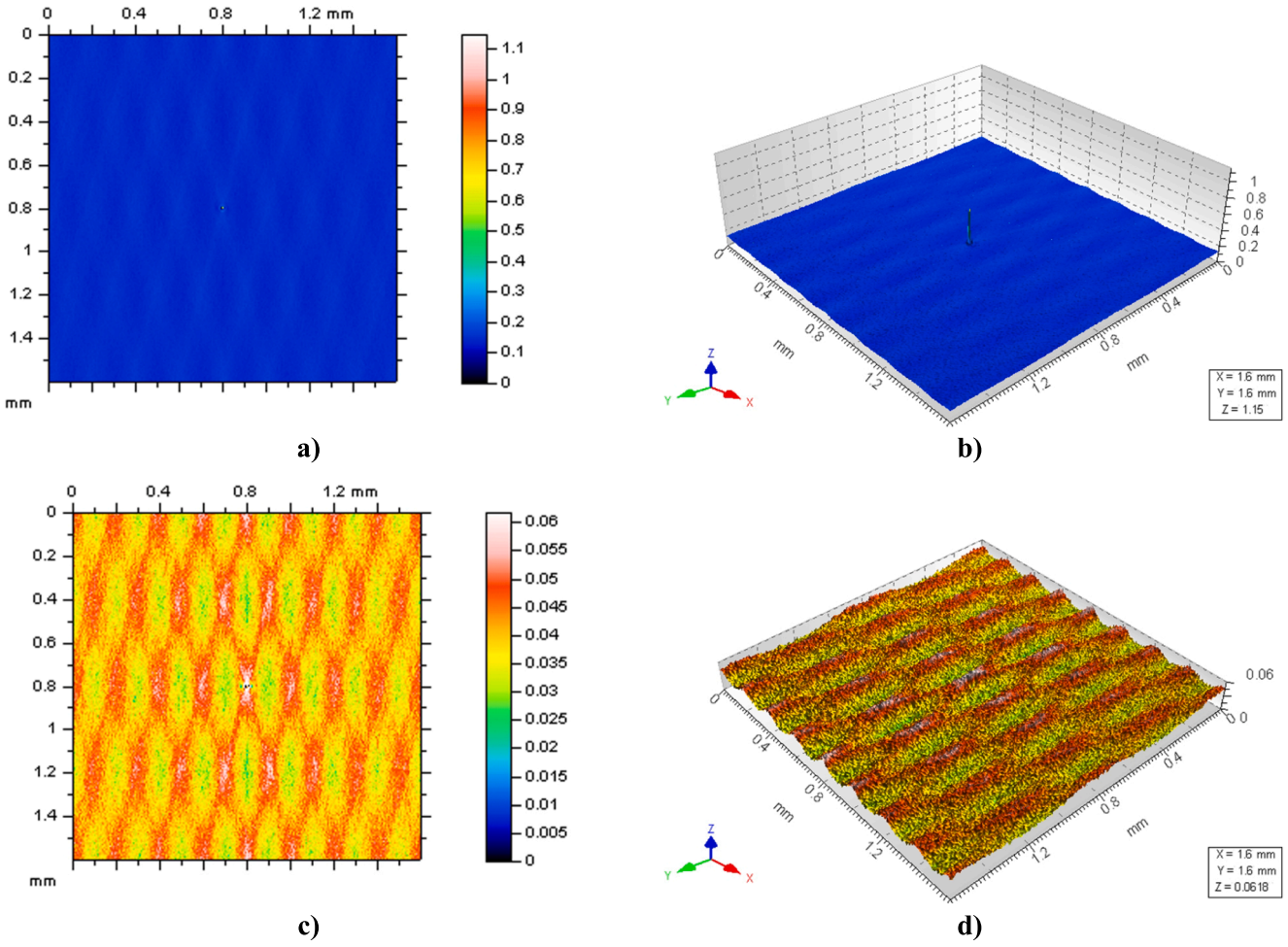

Fig. 6. Contour map plots (a,c) and isometric views (b,d) of ACFs (a,b) and thresholded 0.13 % – 99.87 % ACFs (c,d) calculated for NSs obtained using a 7.5 μm robust Gaussian regression filtering of WLI measured laser-textured cross-hatched surface with an angle (α) of 30°.

the NS data considered the dominant direction, was studied to validate the isotropy properties of the noisy data. In Figs. 10 and 12, the direction of the profile extraction was defined for NS and TD, respectively, with the following angles: $\beta_1 = 134°$ for RGRF, $\beta_2 = 107°$ for SF, $\beta_3 = 89°$ for FFTF, and $\beta_4 = 45°$ for MOF techniques. Considering the profile analysis presented in Fig. 13, the range of the noisy data varied from 0.422 μm to 1.12 μm for the RGRF and SF filtering methods, respectively. The differences in NS profiles are also visible in visual inspection.

Since the NS filtered for the suppression of high-frequency components (measurement noise in this context) should consist of high-frequency data or those data should be dominant, the analysis of profile PSD was conducted in Fig. 13. For the PSD calculated for the NS profile filtered by the RGRF method, two of the three dominant frequencies did not belong to the high-frequency domain. More encouraging results were obtained after FFTF filtration, as two of the three dominant frequencies were within the required frequency range. On the contrary, when applying a MOF technique, all of the first three dominant frequencies were not located in the essential domain. From the four filtering approaches studied, the most promising results were collected when SF was used, with all three dominant frequencies found within the necessary domain. The studied frequencies are indicated in Fig. 13 by the arrows for all four filtering techniques.

The extraction of profiles from the NS in the direction of the dominant frequencies obtained by the TD graph can provide valuable information on the accuracy of the noise-suppression filtering method.

3.2. *Justification of the proposed procedure with the characterisation of variations in ISO 25178 parameters*

In subsequent studies, the effectiveness of the proposed procedure was validated by examining the variations of ISO 25178 surface texture parameters, as presented in Table 1 and Table 2. Among the four proposed filtering techniques, the FFTF method was not studied because the isotropy of NS was equal to 0 % and significant errors were detected in the edge areas of the analysed details.

The influence of the high-frequency errors was evaluated for various types of surface topographies. These results showed similar variations in specific groups of surface texture parameters [68]. The most susceptible parameters to the presence of high-frequency noise were hybrid *Sdq* and *Sdr*, feature *Spc* and *Spd*, and functional *Smr* and *Sk* [69,70]. The influence of the measurement settings on the results of the ISO 25178:600 noise definition [24] and calculation [71] was studied comprehensively in many previous sources [72–75]. However, in our studies, all the ISO 25178 surface texture parameters were divided into two groups: (1) indicators influenced by the presence of high-frequency noise, referred to as 'noise-sensitive'; and (2) parameters partially resilient to the occurrence of the studied type of measurement errors, defined as 'noise-robust'. Previous studies have revealed that noise-sensitive parameters can be distorted more than 100 % in the presence of high-frequency noise while noise-robust parameters show differentiation of less than 5 %. Further studies aimed to compare the differences between these two groups of parameters.

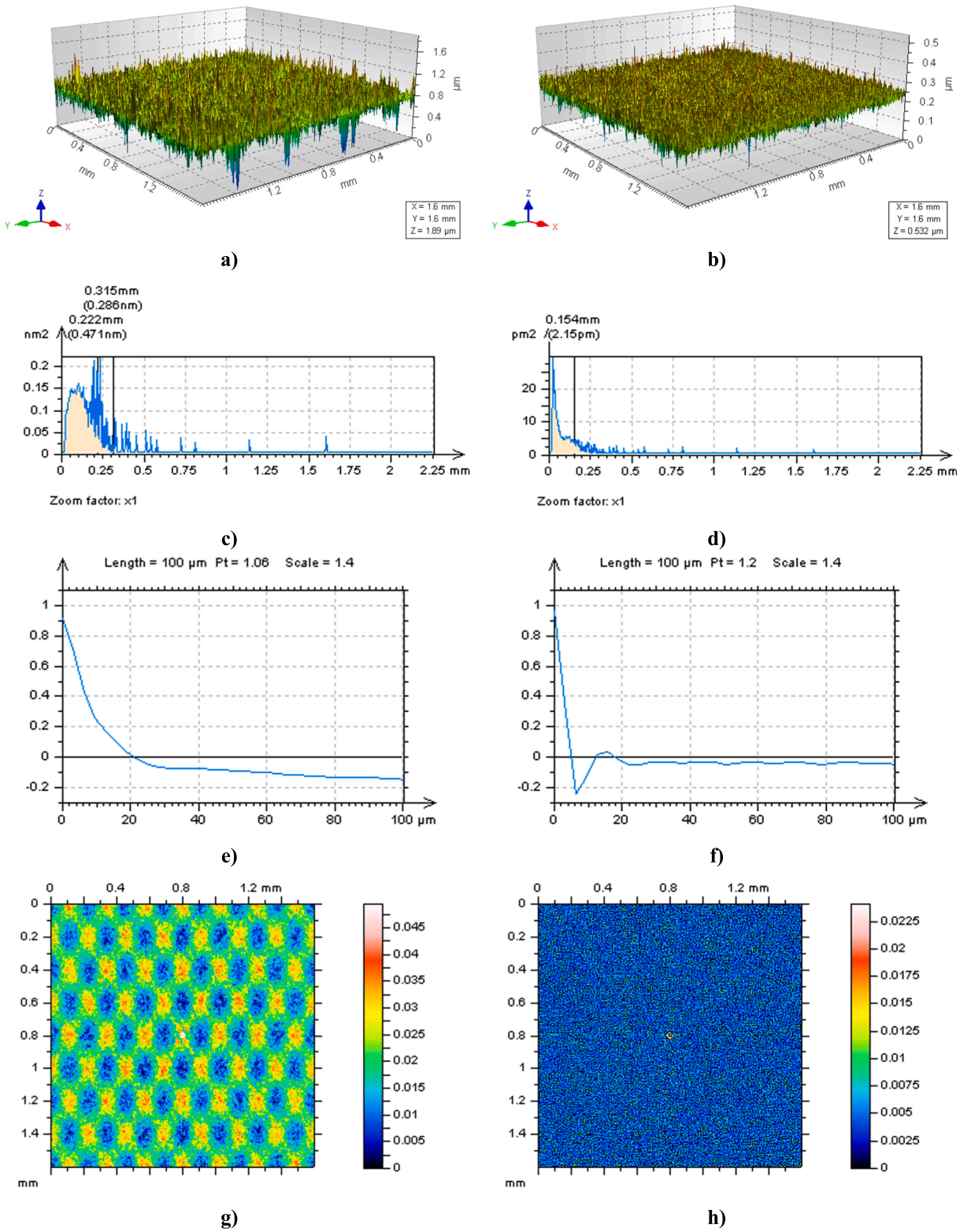

Fig. 7. Isometric views of NSs obtained using a 7.5 µm robust Gaussian regression (a) and a spline (b) filtering technique for a WLI measured laser-textured cross-hatched surface with an angle (α) of 60°, their PSDs (c,d), centre-profile ACFs (e,f) and areal thresholded 0.13 % – 99.87 % ACFs (g,h) characterisations, respectively.

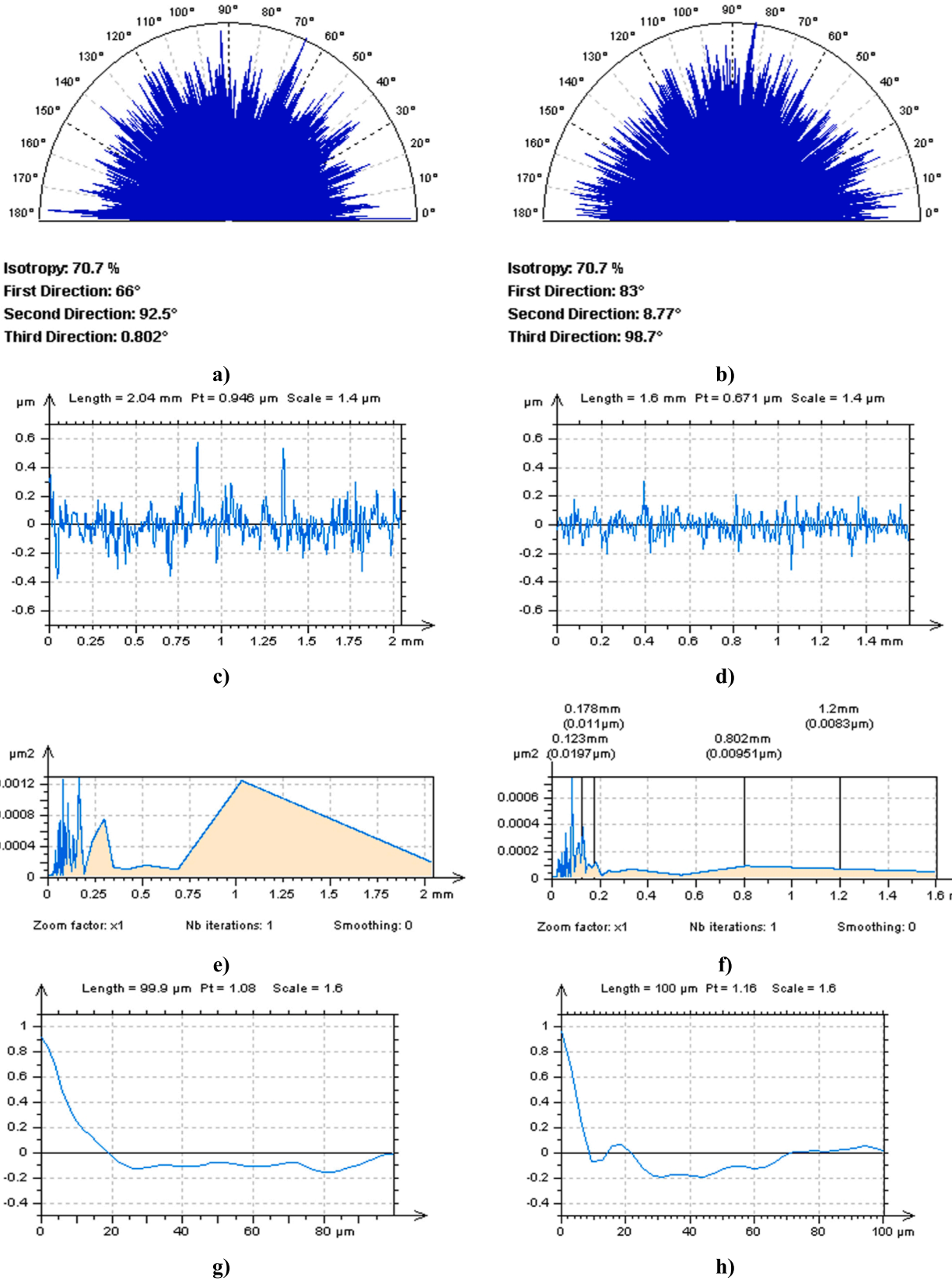

Fig. 8. The TDs graphs of NSs obtained with a 7.5 µm robust Gaussian regression (a) and a spline (b) filtering method for a WLI measured laser-textured cross-hatched surface with an angle (α) of 60°, profiles extracted from NSs in the first TD direction equal to 66° (c) and 83° (d), and their PSDs (e,f) and ACFs (g,h), respectively.

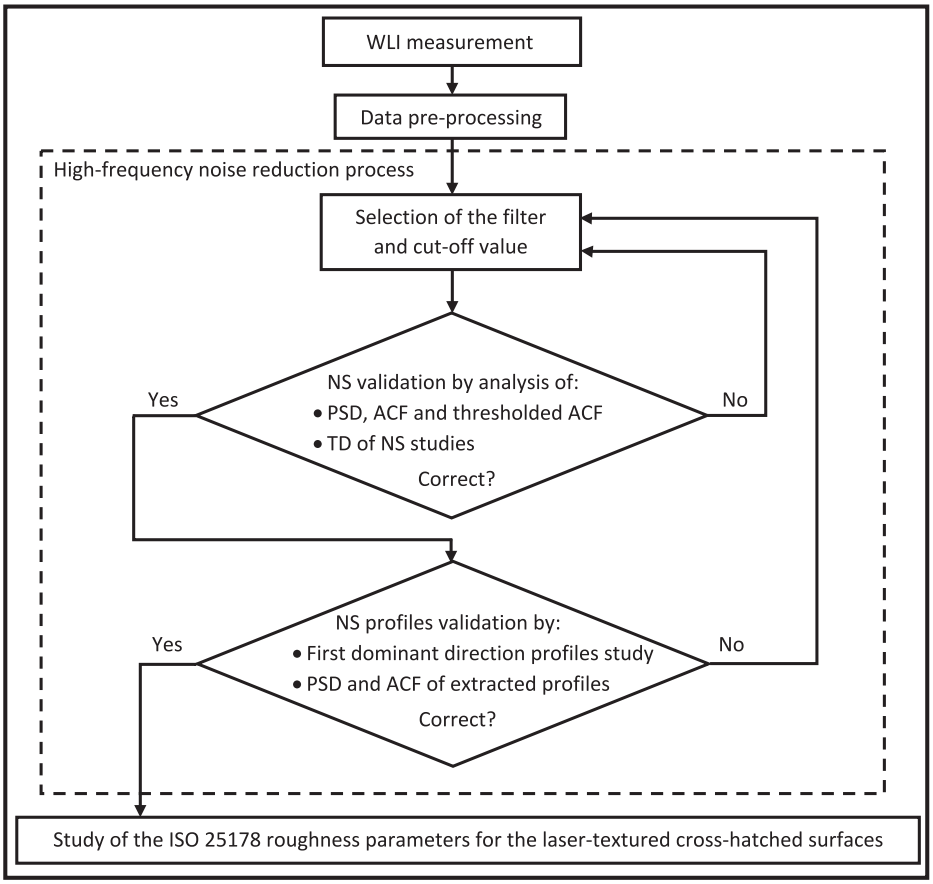

Fig. 9. The flow chart of the proposed procedure.

From the filtering methods, SF gave the lowest values for the functional parameters *Smr* and *Sk* for all four types of cross-hatched surfaces. For the feature parameters, *Spd* and *Spc*, which characterise the peaks of the surface, the differences were generally smaller than 1 %, making it difficult to choose one filter over the others. The hybrid parameters, *Sdq* and *Sdr*, were also minimised when the spline filtering method was used, as opposed to robust Gaussian and morphological techniques.

The final results showed differences depending on the cross-hatch angle value. For $\alpha = 30^\circ$ or $\alpha = 60^\circ$, the advantage of the spline filter over other methods, e.g. robust Gaussian and morphological, was most pronounced. Nevertheless, when α increased, i.e. $\alpha = 120^\circ$ or $\alpha = 150^\circ$, the differences between the spline and robust Gaussian filters decreased by approximately half. Simultaneously, advancements over other methods, such as morphological and fast Fourier filters, increased twice.

Considering the ISO 25178 surface texture parameters, those not classified as vulnerable to variations due to high-frequency measurement noise did not vary more than 10 %, with differences generally smaller than 5 %.

Studying various types of noise-suppression methods, it was proposed to analyse if a particular filter caused variations in noise-sensitive surface texture parameters while maintaining noise-robust parameters unaltered. The application of SF led to the smallest variations in most of the non-noise-sensitive ISO 25178 surface texture parameters.

Based on the findings presented, the SF was classified as the most effective method for reducing high-frequency noise in the results of laser-textured cross-hatched surface topography measurements, considering commonly used filtering techniques, such as robust Gaussian, fast Fourier transform and morphological approaches.

Comparing the proposed methodology to the international standards [24] defining the measurement noise and calculating it with the measurement repeatability [71], the validation was received with the variations of (high-frequency) noise-sensitive ISO 25178 surface texture parameters. The variations of noise-sensitive parameters received from the ISO 25178-700 standard calculations were similar to the variations of ISO 25178 noise-sensitive texture parameters received by the filtering method (and its bandwidth) selected with a proposed methodology.

Due to the root mean square height (*Sq*) of the surface, which is included in the measurement noise calculation formula, can vary depending on the selected area studied, the main line of the method verification was based on the noisy data evaluation, proposed with ACF, PSD and TD characterisation, and study of noise-sensitive surface texture parameters variance. When the measurement noise is known, a proper filter can be applied [76].

From all of the procedures proposed by the ISO 25178-700 standards, the most common method is to repeat the measurement at the same conditions and average the received results [77]. Therefore, according to the validation of the proposal, the results obtained by the application of the filter selected by the new procedure were compared to the average results of three measurements accomplished in the same conditions. The values of noise-sensitive ISO 25178 surface texture parameters were compared to the values of the same noise-sensitive parameters calculated to the average value of 3-time measurement repetitions. The filter with the smallest variations against the averaged results can be classified as the most suitable for the reduction of high-frequency noise. Due to the S-filter proposed by the commercial software, where the regular Gaussian regression filter is used, the new methodology can provide an alternative method for the selection of the high-frequency noise filtering techniques without repeating the measurement process. The validation method for the proposed methodology is presented in Fig. 14.

From the filtering techniques studied, the spline filter caused the most similar variations of the high-frequency measurement noise-

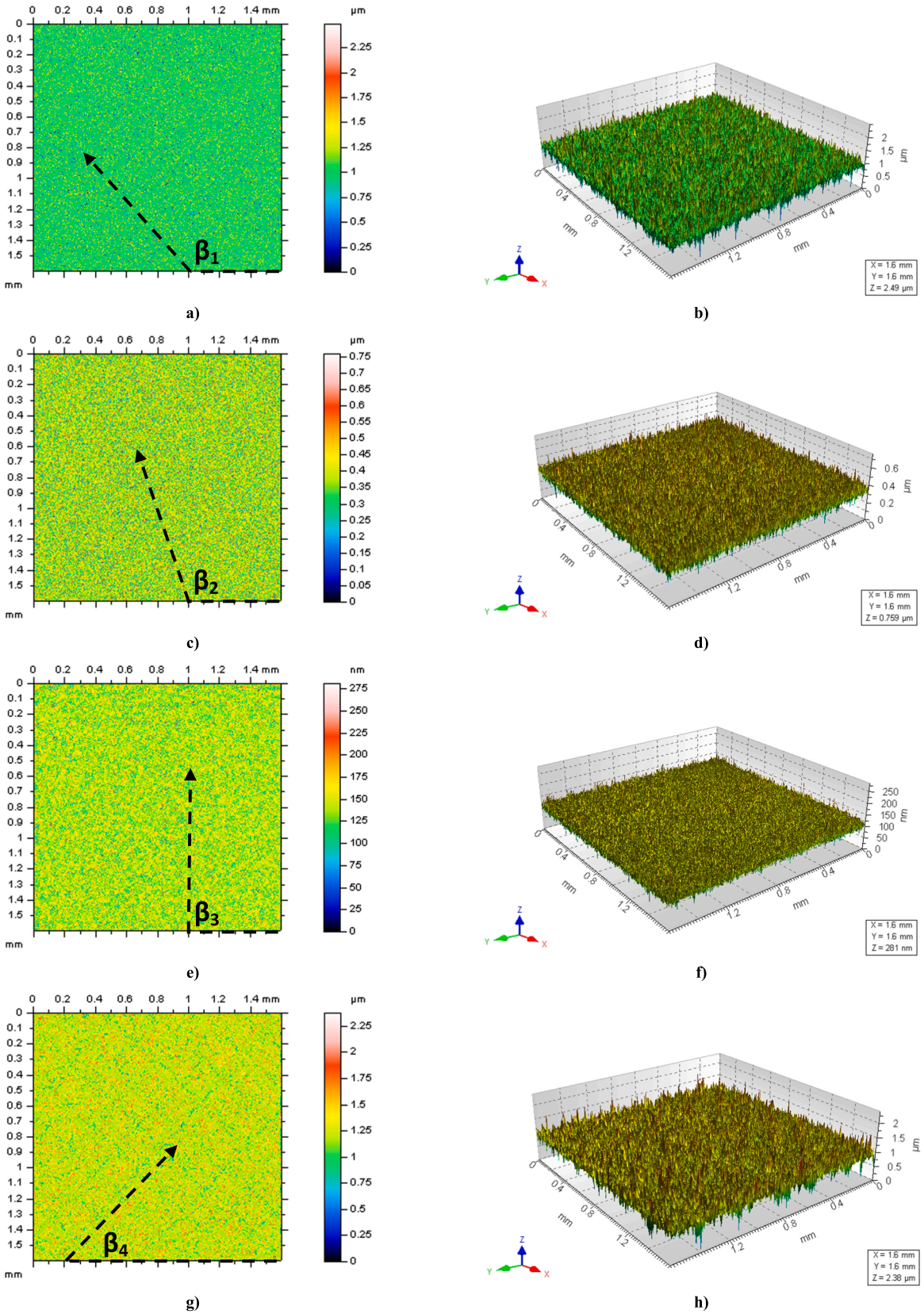

Fig. 10. Contour map plots (a,c,e,g) and isometric views (b,d,f,h) of NSs obtained by the application of RGRF (a,b), SF (c,d), FFTF (e,f) and MOF (g,h) methods for pre-processed data of a WLI measured laser-textured cross-hatched surface with an angle (α) of 90° and cut-off of 7.5 μm; β_1, β_2, β_3 and β_4 are the angles defined for the direction of profile extraction presented in further studies.

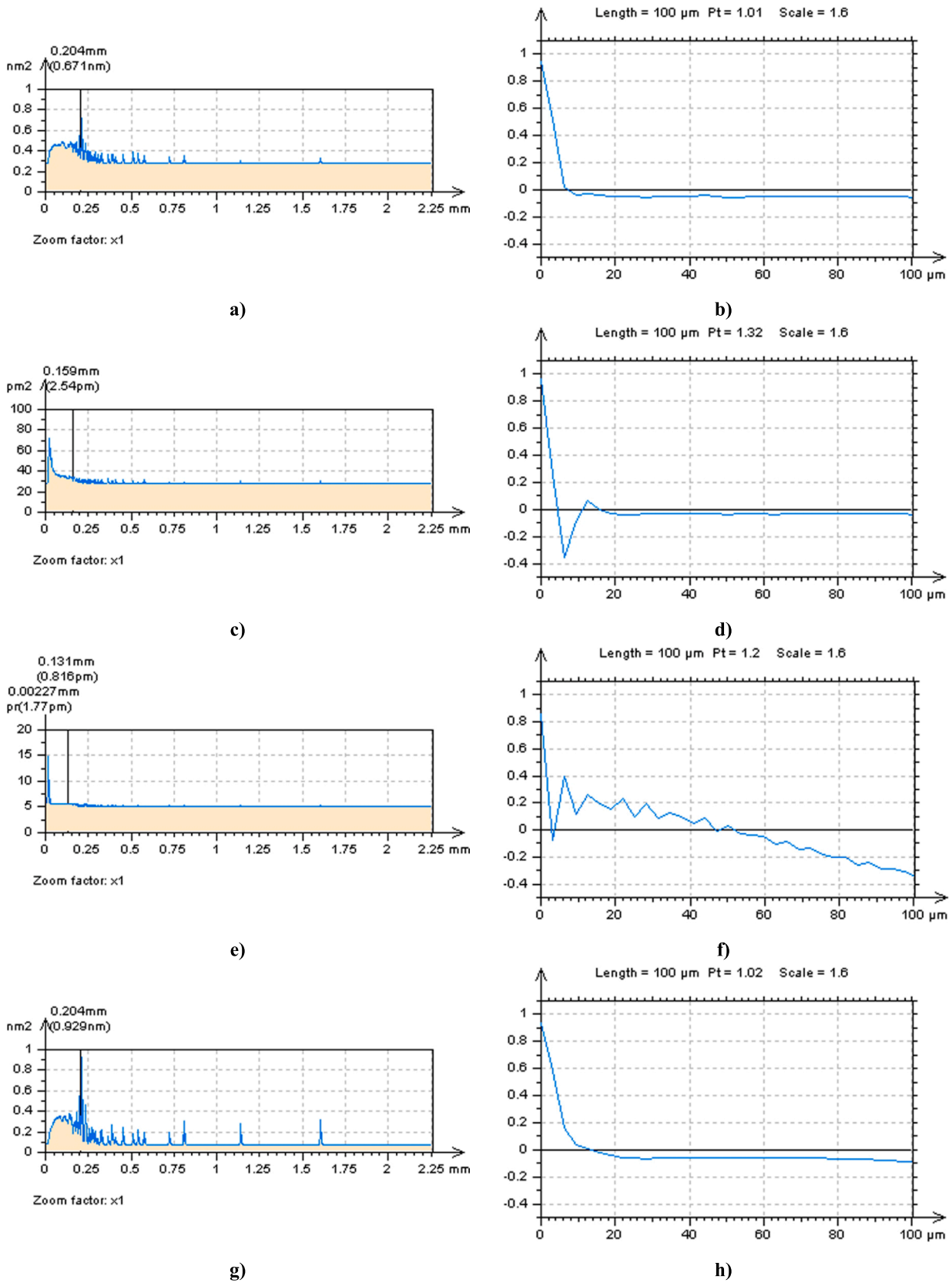

Fig. 11. PSDs (a,c,e,g) and centre-part profiles of ACFs (b,d,f,h) of NSs obtained by the application of RGRF (a,b), SF (c,d), FFTF (e,f) and MOF (g,h) methods for pre-processed data of a WLI measured laser-textured cross-hatched surface with an angle (α) of 90° and cut-off of 7.5 µm.

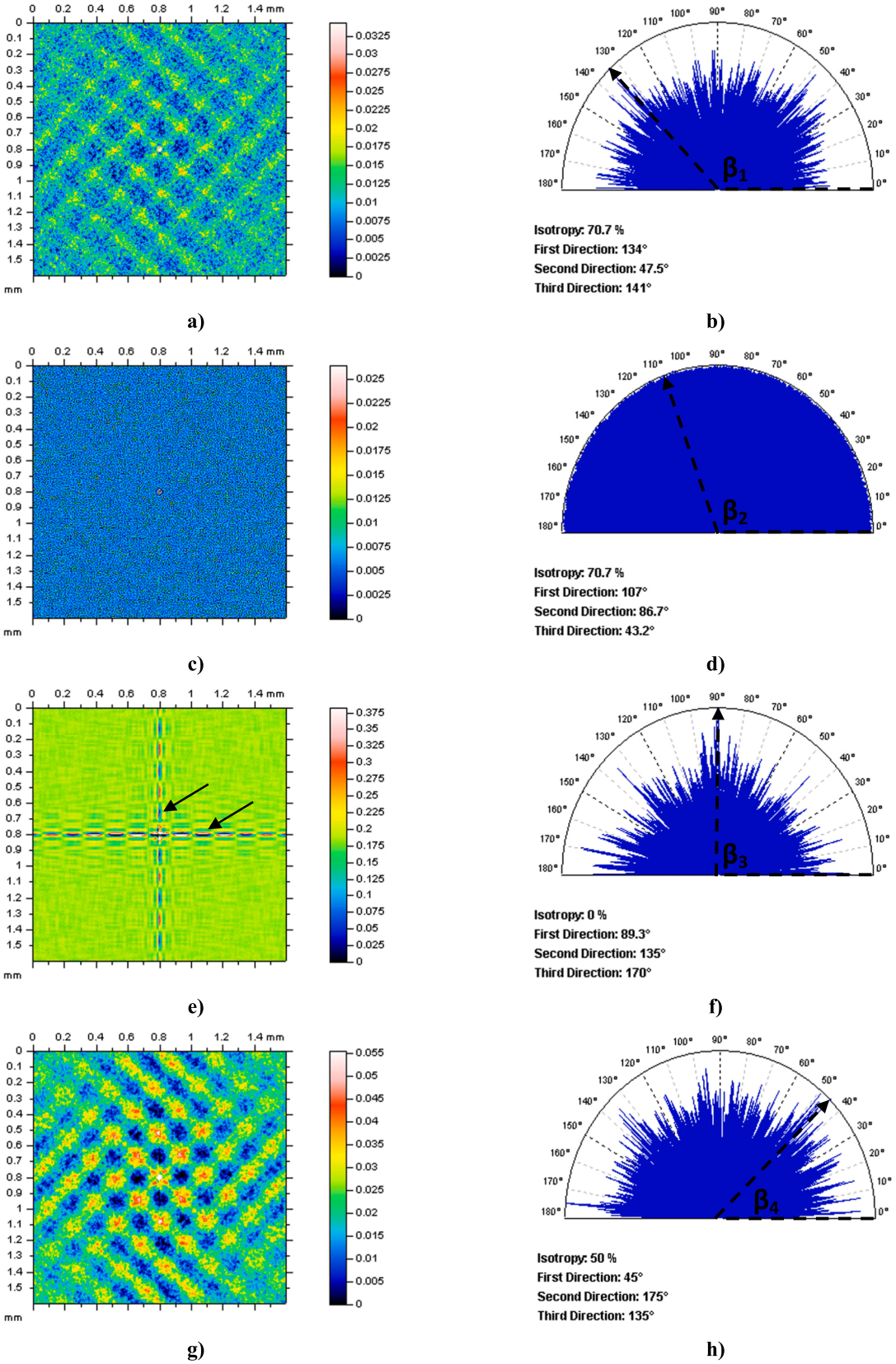

Fig. 12. 0.13 % – 99.87 % thresholded ACFs (a,c,e,g) and TDs (b,d,f,h) of NSs obtained by the application of RGRF (a,b), SF (c,d), FFTF (e,f) and MOF (g,h) methods for pre-processed data of a WLI measured laser-textured cross-hatched surface: $\alpha = 90°$, cut-off = 7.5 μm, $\beta_1 = 134°$, $\beta_2 = 107°$, $\beta_3 = 89°$ and $\beta_4 = 45°$.

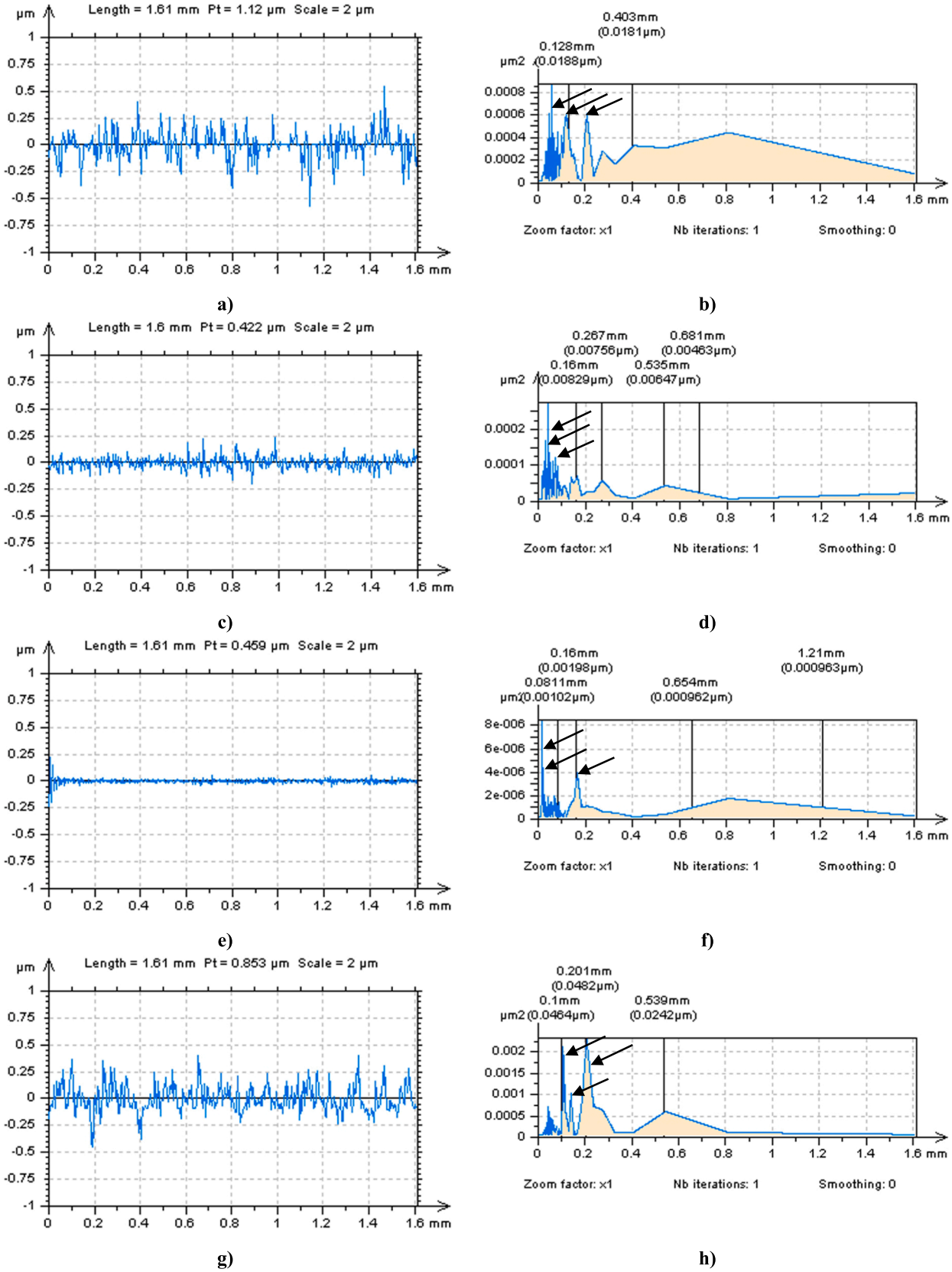

Fig. 13. Profiles (a,c,e,g) and their PSDs (b,d,f,h) extracted from NSs obtained by the application of RGRF (a,b), SF (c,d), FFTF (e,f) and MOF (g,h) methods for pre-processed data of a WLI measured laser-textured cross-hatched surface: $\alpha = 90°$, cut-off = 7.5 µm, the direction of profiles extraction was $\beta_1 = 134°$ (a), $\beta_2 = 107°$ (c), $\beta_3 = 89°$ (e) and $\beta_4 = 45°$ (g).

Table 1
The ISO 25178 surface texture parameters of WLI measured laser-textured cross-hatched surface, calculated for the pre-processed data and data after noise removal by various techniques.

Groups and parameters		Units	$\alpha = 30^\circ$				$\alpha = 60^\circ$			
			Pre-processed	RGRF	SF	MOF	Pre-processed	RGRF	SF	MOF
Height parameters	Sq	μm	1.42	1.40	1.41	1.39	1.41	1.39	1.40	1.38
	Ssk		−0.0173	−0.0274	−0.0187	−0.0334	0.00958	0.00547	0.00901	0.00193
	Sku		2.50	2.48	2.49	2.46	2.63	2.61	2.62	2.6
	Sp	μm	4.88	4.33	4.66	4.02	4.99	4.80	4.87	4.54
	Sv	μm	4.5	4.18	4.28	3.94	4.33	4.24	4.22	3.98
	Sz	μm	9.38	8.51	8.94	7.96	9.32	9.04	9.09	8.53
	Sa	μm	1.16	1.14	1.15	1.13	1.14	1.12	1.13	1.11
Functional parameters	Smr	%	0.0834	0.3870	0.1660	0.8400	0.137	0.269	0.141	0.295
	Smc	μm	3.01	2.48	2.80	2.19	3.15	2.98	3.04	2.73
Spatial parameters	Sal	mm	0.0437	0.0437	0.0437	0.0437	0.0501	0.0501	0.0501	0.0501
	Str		0.261	0.261	0.261	0.261	0.568	0.562	0.567	0.562
	Std	°	76.0	75.9	76.0	76.0	63.5	63.5	63.5	63.5
Hybrid parameters	Sdq		0.0967	0.0676	0.0608	0.0671	0.0956	0.0659	0.0602	0.0647
	Sdr	%	0.467	0.228	0.186	0.238	0.456	0.227	0.205	0.224
Functional parameters (volume)	Vm	mm^3/mm^2	0.0000543	0.0000517	0.0000534	0.0000509	0.0000593	0.0000570	0.0000589	0.0000560
	Vv	mm^3/mm^2	0.0019200	0.0019000	0.0019100	0.0018800	0.0019000	0.0018800	0.0018900	0.0018700
	Vmp	mm^3/mm^2	0.0000543	0.0000517	0.0000534	0.0000509	0.0000593	0.0000570	0.0000589	0.0000560
	Vmc	mm^3/mm^2	0.0013500	0.0013300	0.0013400	0.0013200	0.0013200	0.0013000	0.0013100	0.0013000
	Vvc	mm^3/mm^2	0.0017700	0.0017500	0.0017600	0.0017300	0.0017500	0.0017300	0.0017400	0.0017200
	Vvv	mm^3/mm^2	0.0001520	0.0001510	0.0001510	0.0001500	0.0001540	0.0001510	0.0001530	0.0001500
Feature parameters	Spd	$1/mm^2$	91.5	53.8	53.7	55.8	73.0	43.3	43.0	43.6
	Spc	1/mm	0.0382	0.0197	0.0183	0.0190	0.0382	0.0181	0.0180	0.0182
Functional parameters (stratified surfaces)	Sk	μm	3.94	3.87	3.24	3.84	3.81	3.75	3.69	3.71
	Spk	μm	1.020	0.982	0.997	0.956	1.14	1.09	1.12	1.07
	Svk	μm	1.09	1.07	1.08	1.06	1.14	1.11	1.13	1.11
	Sr1	%	8.58	8.48	8.24	8.46	8.97	9.08	8.99	9.26
	Sr2	%	90.7	90.5	90.6	90.3	90.1	90.0	90.0	90.0
Functional indices	Sbi		0.551	0.675	0.594	0.779	0.525	0.546	0.542	0.598
	Sci		1.53	1.53	1.53	1.52	1.55	1.55	1.55	1.54
	Svi		0.107	0.108	0.107	0.108	0.109	0.109	0.109	0.109

sensitive ISO 25178 texture parameter comparing it to the variations obtained with a calculation of ISO 25178-700 measurement noise with three times of measurement repeatability.

Therefore, the above methodology can be proposed as an alternative and reduce the time-consuming laser-textured surface topography repeatable measurements due to all of the used functions being available in the commercial software of the measuring instrument. Filter and its bandwidth can be quickly selected by calculating the PSD, ACF and TD graphs instead of measurement repetition and average value calculation.

4. Conclusions

Based on the studies presented above, the following conclusions can be drawn:

1. The results of topography measurements of laser-textured cross-hatched surfaces are susceptible to errors related to high-frequency noise. The origin of this type of error is associated with vibrations in the measuring system. Due to the origin of measurement noise in the high-frequency domain is associated with the vibration of the measuring system, the amplitude of the errors can be correlated with the maximum height of the data roughness;
2. The presence of high-frequency errors can cause significant variations in selected ISO 25178 surface texture parameters, namely hybrid root mean square gradient *Sdq* and developed interfacial areal ratio *Sdr*, feature arithmetic mean peak curvature *Spc* and peak density *Spd*, and functional areal material ratio *Smr* and core roughness depth *Sk*. In some cases, variations in surface texture parameter values exceeded 100 %;
3. For the characterisation of high-frequency measurement noise, the autocorrelation function, power spectrum density and texture direction methods can be employed. It was found that advantages in high-frequency noise definition and reduction can be achieved through both areal and profile analyses;
4. Selecting an appropriate filter and its bandwidth analysis for noisy data, also defined as noise surface, being the data removed during

Table 2
The ISO 25178 surface texture parameters of WLI measured laser-textured cross-hatched surface, calculated for the pre-processed data and data after noise removal by various techniques.

Groups and parameters		Units	$\alpha = 90^\circ$				$\alpha = 120^\circ$			
			Pre-processed	RGRF	SF	MOF	Pre-processed	RGRF	SF	MOF
Height parameters	Sq	μm	1.45	1.43	1.44	1.42	1.4	1.37	1.39	1.36
	Ssk		0.01860	0.01450	0.01820	0.00874	−0.00876	−0.01340	−0.00979	−0.01500
	Sku		2.54	2.53	2.53	2.51	2.55	2.53	2.54	2.52
	Sp	μm	4.91	4.68	4.67	4.43	4.82	4.36	4.59	4.13
	Sv	μm	4.23	3.81	4.02	3.64	4.09	4.04	4.00	3.57
	Sz	μm	9.14	8.48	8.69	8.07	8.91	8.40	8.59	7.69
	Sa	μm	1.18	1.16	1.17	1.15	1.14	1.12	1.13	1.11
Functional parameters	Smr	%	0.114	0.171	0.138	0.335	0.0654	0.3470	0.1510	0.7180
	Smc	μm	2.99	2.78	2.76	2.55	2.99	2.55	2.77	2.33
Spatial parameters	Sal	mm	0.0595	0.0595	0.0595	0.0595	0.0501	0.0501	0.0501	0.0501
	Str		0.785	0.785	0.785	0.785	0.554	0.549	0.554	0.549
	Std	°	137	137	137	137	154	154	154	154
Hybrid parameters	Sdq		0.0961	0.0668	0.0680	0.0619	0.0952	0.0651	0.0666	0.0595
	Sdr	%	0.461	0.223	0.231	0.191	0.452	0.212	0.222	0.177
Functional parameters (volume)	Vm	mm^3/mm^2	0.0000586	0.0000569	0.0000579	0.0000558	0.0000564	0.0000546	0.0000557	0.0000536
	Vv	mm^3/mm^2	0.0019800	0.0019500	0.0019700	0.0019300	0.0018900	0.0018600	0.0018800	0.0018500
	Vmp	mm^3/mm^2	0.0000586	0.0000569	0.0000579	0.0000558	0.0000564	0.0000546	0.0000557	0.0000536
	Vmc	mm^3/mm^2	0.0013600	0.0013400	0.0013600	0.0013400	0.0013200	0.0013000	0.0013100	0.0012900
	Vvc	mm^3/mm^2	0.0018200	0.0018000	0.0018200	0.0017800	0.0017400	0.0017100	0.0017300	0.0017000
	Vvv	mm^3/mm^2	0.0001540	0.0001520	0.0001520	0.0001510	0.0001510	0.0001490	0.0001500	0.0001470
Feature parameters	Spd	$1/mm^2$	58.6	37.2	37.5	39.6	76.2	41.7	41.8	42.9
	Spc	1/mm	0.0402	0.0188	0.0190	0.0175	0.0397	0.0187	0.0187	0.0184
Functional parameters (stratified surfaces)	Sk	μm	3.98	3.95	3.95	3.89	3.81	3.75	3.80	3.71
	Spk	μm	1.13	1.08	1.11	1.07	10.7	1.05	1.06	1.03
	Svk	μm	1.11	1.09	1.11	1.08	1.09	1.07	1.09	1.06
	Sr1	%	9.27	8.81	9.25	9.07	8.96	8.87	8.69	8.86
	Sr2	%	90.9	90.7	90.8	90.6	90.2	90.2	90.2	90.0
Functional indices	Sbi		0.579	0.615	0.63	0.679	0.552	0.654	0.598	0.715
	Sci		1.57	1.56	1.57	1.56	1.55	1.55	1.55	1.54
	Svi		0.107	0.107	0.106	0.107	0.108	0.108	0.108	0.108

noise-suppression filtering, can be especially beneficial. It is crucial that the noise surface is isotropic and does not contain non-noise features;

5. Comprehensive studies of noise surfaces, particularly based on profiles extracted in the direction of the machining process, can enhance the noise-removal procedure. It is recommended to use the dominant direction calculated from the texture direction function for the characterisation of noise surface properties. A suitable defined noise surface, indicative of the application of a well-chosen filter and its cut-off value, should contain profiles with a similar frequency composition, as determined with a spectral analysis;
6. Errors in the calculation of ISO 25178 surface texture parameters caused by the presence of high-frequency measurement noise, can be reduced through data filtering using the proposed procedure. The proposed procedure was validated from laser-textured surfaces with varying cross-hatched angles equal to 30°, 60°, 90°, 120° and 150°;
7. For laser-textured cross-hatched surfaces, the 7.5 μm regular isotropic spline filter led to the most promising results considering all the filtering methods studied. Variations in the values of surface texture parameters susceptible to high-frequency noise were minimised when compared to the application of robust Gaussian regression, fast Fourier transforms and envelope-closing-opening morphological filters when the proposed procedure was applied.

CRediT authorship contribution statement

Przemysław Podulka: Writing – original draft, Visualization, Validation, Software, Resources, Methodology, Investigation, Formal analysis, Data curation, Conceptualization. **Wojciech Macek:** Writing – review & editing, Validation, Supervision, Software, Resources, Formal analysis. **Ricardo Branco:** Software, Supervision, Visualization, Writing – review & editing. **Andrzej Kubit:** Writing – review & editing, Visualization, Validation, Supervision, Software.

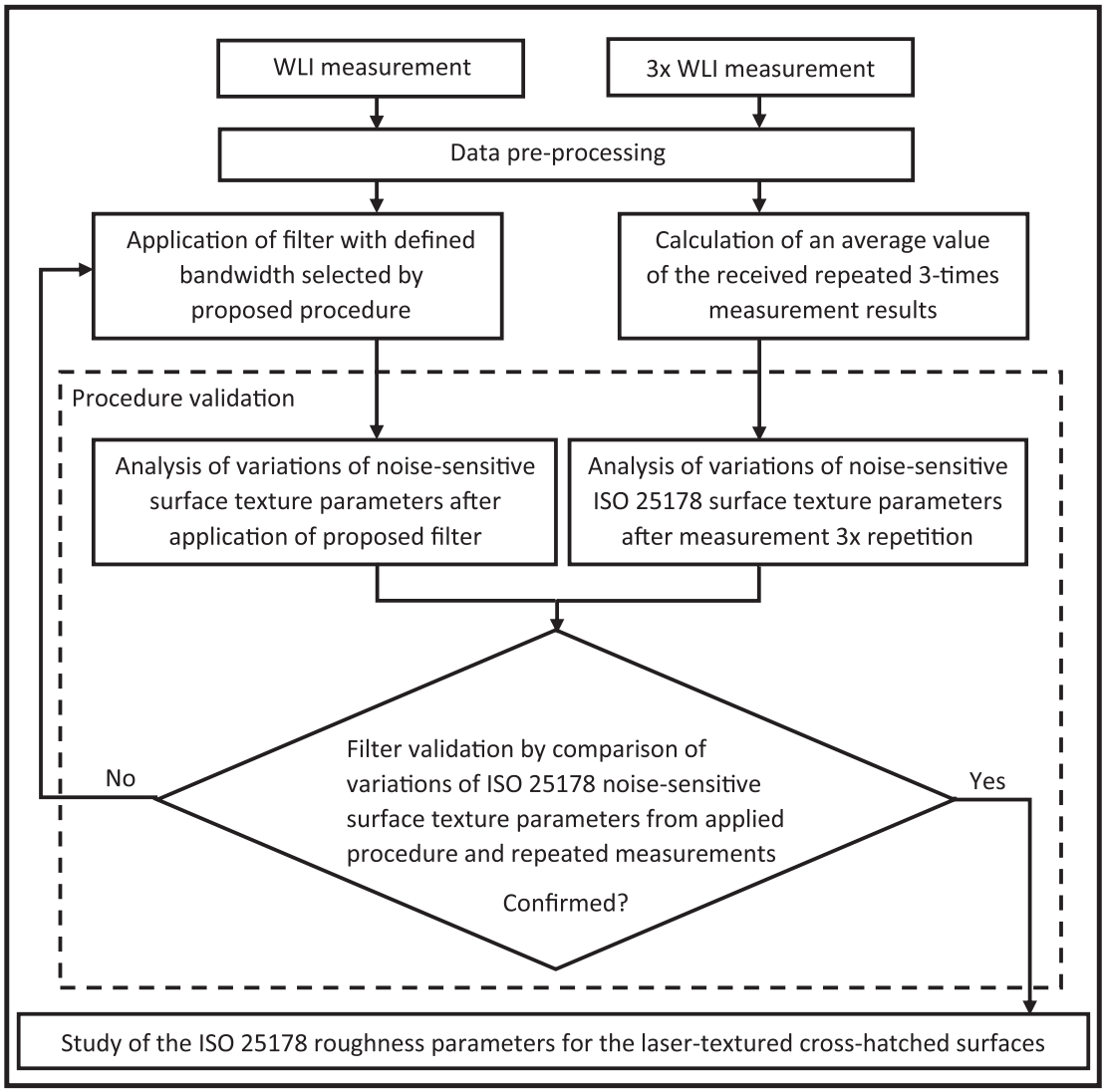

Fig. 14. The flow chart of the methodology validation method.

Declaration of competing interest

The authors declare that they have no known competing financial interests or personal relationships that could have appeared to influence the work reported in this paper.

Data availability

Data will be made available on request.

Acknowledgement

This research is sponsored by national funds through FCT – Fundação para a Ciência e a Tecnologia, under the project UIDB/00285/2020 and LA/P/0112/2020.

References

[1] Y. Shao, F. Xu, J. Chen, J. Lu, S. Du, Engineering surface topography analysis using an extended discrete modal decomposition, J. Manuf. Process. 90 (2023) 367–390, https://doi.org/10.1016/j.jmapro.2023.02.005.
[2] M. Szpunar, T. Trzepieciński, K. Żaba, R. Ostrowski, M. Zwolak, Effect of lubricant type on the friction behaviours and surface topography in metal forming of Ti-6Al-4V titanium alloy sheets, Materials 14 (2021) 3721, https://doi.org/10.3390/ma14133721.
[3] T. Trzepieciński, R. Fejkiel, On the influence of deformation of deep drawing quality steel sheet on surface topography and friction, Tribol. Int. 115 (2017) 78–88, https://doi.org/10.1016/j.triboint.2017.05.007.
[4] B. Bussière, N. Sanner, M. Sentis, O. Utéza, Importance of surface topography on pulsed laser-induced damage threshold of Sapphire crystals, Sci. Rep. 7 (2017) 1249, https://doi.org/10.1038/s41598-017-01192-7.
[5] W. Macek, D. Rozumek, G.M. Królczyk, Surface topography analysis based on fatigue fractures obtained with bending of the 2017A–T4 alloy, Measurement 152 (2020) 107347, https://doi.org/10.1016/j.measurement.2019.107347.
[6] D.E. Zakrzewska, M.H. Buszko, A. Marchewicz, A.K. Krella, Concept of cavitation erosion assessment of austenitic 1.4301 stainless steel based on roughness development, Tribol. Int. 183 (2023) 108431, https://doi.org/10.1016/j.triboint.2023.108431.
[7] Y. Zhang, C. Zhou, H. Feng, A meticulous friction torque model for a lubricated ball screw considering the surface roughness, Tribol. Int. 190 (2023) 109014, https://doi.org/10.1016/j.triboint.2023.109014.
[8] S. Reichert, B. Lorentz, S. Heldmaier, A. Albers, Wear simulation in non-lubricated and mixed lubricated contacts taking into account the microscale roughness, Tribol. Int. 100 (2016) 272–279, https://doi.org/10.1016/j.triboint.2016.02.009.
[9] P. Pawlus, R. Reizer, M. Wieczorowski, Characterization of the shape of height distribution of two-process profile, Measurement 153 (2020) 107387–107395, https://doi.org/10.1016/j.measurement.2019.107387.
[10] I. Etsion, State of the art in laser surface texturing, J. Tribol.-Trans. ASME 127 (2005) 248–253, https://doi.org/10.1115/1.1828070.
[11] D.S. Patel, A. Singh, K. Balani, J. Ramkumar, Topographical effects of laser surface texturing on various time-dependent wetting regimes in Ti6Al4V, Surf. Coat. Technol. 349 (2018) 816–829, https://doi.org/10.1016/j.surfcoat.2018.05.032.
[12] A. Riveiro, A.L.B. Maçon, J. del Val, R. Comesaña, J. Pou, Laser surface texturing of polymers for biomedical applications, Front. Phys. 6 (2018) 16, https://doi.org/10.3389/fphy.2018.00016.

[13] J.A. Wahab, M.J. Ghazali, W.M.W. Yusoff, Z. Sajuri, Enhancing material performance through laser surface texturing: a review, Trans. Inst. Met. Finish. 94 (2016) 193–198, https://doi.org/10.1080/00202967.2016.1191141.
[14] S. Fang, L. Llanes, D. Bähre, Laser surface texturing of a WC-CoNi cemented carbide grade: surface topography design for honing application, Tribol. Int. 122 (2018) 236–245, https://doi.org/10.1016/j.triboint.2018.02.018.
[15] A.A. Voevodin, J.S. Zabinski, Laser surface texturing for adaptive solid lubrication, Wear 261 (11–12) (2006) 1285–1292, https://doi.org/10.1016/j.wear.2006.03.013.
[16] A.H.A. Lutey, L. Romoli, Surface topography following pulsed laser texturing: implications for adhesion and wettability, Surf. Topogr. Metrol. Prop. 7 (4) (2019) 045023, https://doi.org/10.1088/2051-672X/ab5c82.
[17] I. Shivakoti, G. Kibria, R. Cep, B.B. Pradhan, A. Sharma, Laser surface texturing for biomedical applications: a review, Coatings 11 (2021) 124, https://doi.org/10.3390/coatings11020124.
[18] L. Tiainen, P. Abreu, M. Buciumeanu, F. Silva, M. Gasik, C.O. Guerrero, Novel laser surface texturing for improved primary stability of titanium implants, J. Mech. Behav. Biomed. Mater. 98 (2019) 26–39, https://doi.org/10.1016/j.jmbbm.2019.04.052.
[19] W. Cunha, O. Carvalho, B. Henriques, F.S. Silva, M. Özcan, J.C.M. Souza, Surface modification of zirconia dental implants by laser texturing, Lasers Med. Sci. 37 (2022) 77–93, https://doi.org/10.1007/s10103-021-03475-y.
[20] M. Khatami, Laser nano surface texturing for enhancing of physical and chemical properties of dental implants, Nanomed. Res. J. 8 (2023) 1–15, https://doi.org/10.22034/nmrj.2023.01.001.
[21] S. Mukherjee, S. Dhara, P. Saha, Enhancing the biocompatibility of Ti6Al4V implants by laser surface microtexturing: an in vitro study, Int. J. Adv. Manuf. Technol. 76 (2015) 5–15, https://doi.org/10.1007/s00170-013-5277-2.
[22] C. Hallgren, H. Reimers, J. Gold, A. Wennerberg, The importance of surface texture for bone integration of screw shaped implants: an in vivo study of implants patterned by a photolithography technique, J. Biomed. Mater. Res. 57 (2001) 485–496, https://doi.org/10.1002/1097-4636(20011215)57:4%3C485::AID-JBM1194%3E3.0.CO;2-1.
[23] G. Menci, A.G. Demir, D.G. Waugh, J. Lawrence, B. Previtali, Laser surface texturing of β-Ti alloy for orthopaedics: effect of different wavelengths and pulse durations, Appl. Surf. Sci. 489 (2019) 175–186, https://doi.org/10.1016/j.apsusc.2019.05.111.
[24] ISO 25178-600, Geometric Product Specifications (GPS)–Surface texture: Areal – Part 600: Metrological characteristics for areal topography measuring instruments, International Organization for Standardization, Geneva, Switzerland, 2019.
[25] P. De Groot, J. DiSciacca, Definition and evaluation of topography measurement noise in optical instruments, Opt. Eng. 59 (2020) 064110, https://doi.org/10.1117/1.OE.59.6.064110.
[26] C.L. Giusca, R.K. Leach, F. Helary, T. Gutauskas, L. Nimishakavi, Calibration of the scales of areal surface topography-measuring instruments: Part 1. Measurement noise and residual flatness, Meas. Sci. Technol. 23 (2012) 035008, https://doi.org/10.1088/0957-0233/23/3/035008.
[27] Z. Yao, J. Shen, M. Wu, D. Zhang, M. Luo, Position-dependent milling process monitoring and surface roughness prediction for complex thin-walled blade component, Mech. Syst. Sig. Process. 198 (2023) 110439, https://doi.org/10.1016/j.ymssp.2023.110439.
[28] P. Podulka, Improved procedures for feature-based suppression of surface texture high-frequency measurement errors in the wear analysis of cylinder liner topographies, Metals 11 (2021) 143, https://doi.org/10.3390/met11010143.
[29] O.V. Zakharov, A.S. Yakovishin, A.V. Zhukov, Robustness analysis of Gaussian filters for surface texture of additive manufacturing products, in: 2022 International Russian Automation Conference (RusAutoCon), Sochi, Russian Federation, 2022, 28–33. https://www.doi.org/10.1109/RusAutoCon54946.2022.9896266.
[30] Y.B. Yuan, X.F. Qiang, J.F. Song, T. Vorburger, A fast algorithm for determining the Gaussian filtered mean line in surface metrology, Precis. Eng. 24 (2000) 62–69, https://doi.org/10.1016/S0141-6359(99)00031-8.
[31] ISO 16610-61:2015, Geometrical Product Specification (GPS)—Filtration—Part 61: Linear Areal Filters—Gaussian Filters; ISO: Geneva, Switzerland, 2015.
[32] N.L. Luo, P.J. Sullivan, K.J. Stout, Gaussian filtering of three-dimensional engineering surface topography, Measur. Technol. Intel. Instrum. Int. Soc. Opt. Photon. 2101 (1993) 527–538, https://doi.org/10.1117/12.156497.
[33] P. Dobrzański, P. Pawlus, Modification of robust filtering of stratified surface topography, Metrol. Measur. Syst. 20 (2013) 107–118, https://doi.org/10.2478/mms-2013-0010.
[34] H.Q. Chen, Q.H. Wang, Modeling and simulation of the surface topography in ball-end milling based on biharmonic spline interpolation, Int. J. Adv. Manuf. Technol. 99 (2018) 2451–2466, https://doi.org/10.1007/s00170-018-2615-4.
[35] P. Podulka, Suppression of the high-frequency errors in surface topography measurements based on comparison of various spline filtering methods, Materials 14 (2021) 5096, https://doi.org/10.3390/ma14175096.
[36] D. Janecki, A two-dimensional isotropic spline filter, Precis. Eng. 37 (2013) 948–965, https://doi.org/10.1016/j.precisioneng.2013.05.005.
[37] M. Tong, H. Zhang, D. Ott, W. Chu, J. Song, Applications of the spline filter for areal filtration, Meas. Sci. Technol. 26 (2015) 127002, https://doi.org/10.1088/0957-0233/26/12/127002.
[38] D. Gogolewski, Fractional spline wavelets within the surface texture analysis, Measurement 179 (2021) 109435, https://doi.org/10.1016/j.measurement.2021.109435.
[39] Y.F. He, J.Y. Tang, W. Zhou, D.R. Liao, Research on the obtainment of topography parameters by rough surface simulation with fast Fourier transform, J. Tribol.-Trans. ASME 137 (3) (2015) 031401, https://doi.org/10.1115/1.4029843.
[40] C.L. Tien, H.M. Yang, M.C. Liu, The measurement of surface roughness of optical thin films based on fast Fourier transform, Thin Solid Films 517 (17) (2009) 5110–5115, https://doi.org/10.1016/j.tsf.2009.03.193.
[41] Y. Jiang, S. Wang, H. Qin, B. Li, Q. Li, Similarity quantification of 3D surface topography measurements, Measurement 186 (2021) 110207, https://doi.org/10.1016/j.measurement.2021.110207.
[42] Y. Dong, Z. Li, L. Zhu, X. Zhang, Topography measurement and reconstruction of inner surfaces based on white light interference, Measurement 186 (2021) 110199, https://doi.org/10.1016/j.measurement.2021.110199.
[43] P. Podulka, Fast Fourier Transform detection and reduction of high-frequency errors from the results of surface topography profile measurements of honed textures, Eksploatacja i Niezawodnosc-Maintenance Reliabil. 23 (2021) 84–93, https://doi.org/10.17531/ein.2021.1.9.
[44] R. Guo, Z. Liao, J. Li, A. Li, P. Song, R. Zhu, Optical homogeneity measurement of parallel plates by wavelength-tuning interferometry using nonuniform fast Fourier transform, Opt. Express 27 (2019) 13072–13082, https://doi.org/10.1364/OE.27.013072.
[45] ISO 16610-85:2013, Geometrical product specifications (GPS) — Filtration — Part 85: Morphological areal filters: Segmentation; ISO: Geneva, Switzerland, 2013.
[46] S. Lou, X. Jiang, P.J. Scott, Application of the morphological alpha shape method to the extraction of topographical features from engineering surfaces, Measurement 46 (2013) 1002–1008, https://doi.org/10.1016/j.measurement.2012.09.015.
[47] M.Y. Zakharchenko, A.V. Kochetkov, P.M. Salov, O.V. Zakharov, New system of functional parameters for surface texture analysis, Mater. Today:. Proc. 38 (4) (2021) 1866–1870, https://doi.org/10.1016/j.matpr.2020.08.488.
[48] S. Lou, X. Jiang, P.J. Bills, P.J. Scott, Defining true tribological contact through application of the morphological method to surface topography, Tribol. Lett. 50 (2013) 185–193, https://doi.org/10.1007/s11249-013-0111-4.
[49] L. Newton, N. Senin, B. Smith, E. Chatzivagiannis, R. Leach, Comparison and validation of surface topography segmentation methods for feature-based characterisation of metal powder bed fusion surfaces, Surf. Topogr. Metrol. Prop. 7 (2019) 045020, https://doi.org/10.1088/2051-672X/ab520a.
[50] D. Lipiński, W. Kacalak, Metrological aspects of abrasive tool active surface topography evaluation, Metrol. Measur. Syst. 23 (2016) 567–577, https://doi.org/10.1515/mms-2016-0043.
[51] P. Podulka, Comparisons of envelope morphological filtering methods and various regular algorithms for surface texture analysis, Metrol. Measur. Syst. 27 (2020) 243–263, https://doi.org/10.24425/mms.2020.132772.
[52] M. Organisciak, G. Cavallaro, A.A. Lubrecht, Influence of the cross-hatched surface texture on a starved hydrodynamic linear contact, in: Proceedings of the ASME/STLE 2007 international joint tribology conference, parts A and B, San Diego, 2007, pp. 905–907, https://doi.org/10.1115/ijtc2007-44144.
[53] S. Ozan, A. Bilgin, Ş. Kasman, Laser textured Ti-6Al-7Nb alloy for biomedical applications: an investigation of texturing parameters on surface properties, Proc. Inst. Mech. Eng., H: J. Eng. Med. (2023), https://doi.org/10.1177/09544119231200537.
[54] B. Guimarães, C.M. Fernandes, D. Figueiredo, O. Carvalho, F.S. Silva, G. Miranda, Effect of laser surface texturing on the wettability of WC-Co cutting tools, Int. J. Adv. Manuf. Technol. 111 (2020) 1991–1999, https://doi.org/10.1007/s00170-020-06155-3.
[55] M. Conradi, T. Kosec, B. Podgornik, A. Kocijan, J. Kovač, D. Klobčar, Effect of laser texturing pattern on Ti6Al4V tribo-corrosion in a physiological solution, Surf. Innovations 10 (2022) 11, https://doi.org/10.1680/jsuin.21.00048.
[56] M. Conradi, A. Kocijan, D. Klobčar, B. Podgornik, Tribological response of laser-textured Ti6Al4V alloy under dry conditions and lubricated with Hank's solution, Tribol. Int. 160 (2021) 107049, https://doi.org/10.1016/j.triboint.2021.107049.
[57] D. Madapana, R. Bathe, I. Manna, J.D. Majumdar, Chemical and mechanochemical degradations of ultrafast laser surface structured Ti6Al4V in simulated body fluid environment, Appl. Surf. Sci. 649 (2024) 159096, https://doi.org/10.1016/j.apsusc.2023.159096.
[58] L. Giorleo, L. Montesano, G.M. La Vecchia, Laser surface texturing to realize micro-grids on DLC coating: effect of marking speed, power, and loop cycle, Int. J. Precis. Eng. Manuf. 22 (2022) 745–758, https://doi.org/10.1007/s12541-021-00498-x.
[59] P. Podulka, P. Pawlus, P. Dobrzański, A. Lenart, Spikes removal in surface measurement, J. Phys. Conf. Ser. 483 (2014) 012025, https://doi.org/10.1088/1742-6596/483/1/012025.
[60] P. Podulka, W. Macek, B. Zima, G. Lesiuk, R. Branco, G.M. Królczyk, Roughness evaluation of turned composite surfaces by analysis of the shape of autocorrelation function, Measurement 222 (2023) 113640, https://doi.org/10.1016/j.measurement.2023.113640.
[61] P. Podulka, W. Macek, R. Branco, R.M. Nejad, Reduction in errors in roughness evaluation with an accurate definition of the S-L surface, Materials 2023 (1865) 16, https://doi.org/10.3390/ma16051865.
[62] T.D.B. Jacobs, T. Junge, L. Pastewka, Quantitative characterization of surface topography using spectral analysis, Surf. Topogr. Metrol. Prop. 5 (2017) 013001, https://doi.org/10.1088/2051-672X/aa51f8.
[63] S.G. Alcock, G.D. Ludbrook, T. Owen, R. Dockree, Using the power spectral density method to characterise the surface topography of optical surfaces, Proc. SPIE 7801 (2010) 780108, https://doi.org/10.1117/12.861539.
[64] M. Uchidate, T. Shimizu, A. Iwabuchi, K. Yanagi, Generation of reference data of 3D surface texture using the non-causal 2D AR model, Wear 257 (12) (2004) 1288–1295, https://doi.org/10.1016/j.wear.2004.05.019.

[65] P. Podulka, Resolving selected problems in surface topography analysis by application of the autocorrelation function, Coatings 13 (2023) 74, https://doi.org/10.3390/coatings13010074.
[66] P. Pawlus, Simulation of stratified surface topographies, Wear 264 (2008) 457–463, https://doi.org/10.1016/j.wear.2006.08.048.
[67] M. Niemczewska-Wójcik, Multi-sensor measurements of titanium alloy surface texture formed at subsequent operations of precision machining process, Measurement 96 (2017) 8–17, https://doi.org/10.1016/j.measurement.2016.10.049.
[68] P. Podulka, Reduction of influence of the high-frequency noise on the results of surface topography measurements, Materials 14 (2021) 333, https://doi.org/10.3390/ma14020333.
[69] P. Pawlus, R. Reizer, M. Wieczorowski, G.M. Królczyk, Study of surface texture measurement errors, Measurement 210 (2023) 112568, https://doi.org/10.1016/j.measurement.2023.112568.
[70] P. Podulka, W. Macek, D. Rozumek, K. Żak, R. Branco, Topography measurement methods evaluation for entire bending-fatigued fracture surfaces of specimens obtained by explosive welding, Measurement 224 (2024) 113853, https://doi.org/10.1016/j.measurement.2023.113853.
[71] ISO 25178-700:2022. Geometrical product specifications (GPS) Surface texture: Areal Part 700: Calibration, adjustment and verification of areal topography measuring instruments. International Organization for Standardization, Geneva, Switzerland, 2022.
[72] Z. Li, S. Gröger, Investigation of noise in surface topography measurement using structured illumination microscopy, Metrol. Meas. Syst. 28 (2021) 4, https://doi.org/10.24425/mms.2021.137706.
[73] M. Eifler, J. Hering, J. Seewing, R.K. Leach, G. von Freymann, X. Hu, G. Dai, Comparison of material measures for areal surface topography measuring instrument calibration, Surf. Topogr. Metrol. Prop. 8 (2020) 025019, https://doi.org/10.1088/2051-672X/ab92ae.
[74] M. Vanrusselt, H. Haitjema, R.K. Leach, P. de Groot, International comparison of noise in areal surface topography measurements, Surf. Topogr. Metrol. Prop. 9 (2021) 025015, https://doi.org/10.1088/2051-672X/abfa29.
[75] A. Pappas, L. Newton, R.K. Leach, Review of material measures for surface topography instrument calibration and performance verification, Meas. Sci. Technol. 35 (2023) 012001, https://doi.org/10.1088/1361-6501/acf1b9.
[76] P. Pawlus, R. Reizer, M. Wieczorowski, G.M. Krolczyk, Sensitivities of surface texture parameters to measurement errors – a review, Measurement 227 (2024) 114323, https://doi.org/10.1016/j.measurement.2024.114323.
[77] K. Peta, G. Love, C.A. Brown, Comparing repeatability and reproducibility of topographic measurement types directly using linear regression analyses of measured heights, Precis. Eng. 88 (2024) 192–203, https://doi.org/10.1016/j.precisioneng.2024.02.009.